



HAL
open science

A comparison of eight weakly dispersive Boussinesq-type models for non-breaking long-wave propagation in variable water depth

Guillaume Coulaud, Maria Teles, Michel Benoit

► To cite this version:

Guillaume Coulaud, Maria Teles, Michel Benoit. A comparison of eight weakly dispersive Boussinesq-type models for non-breaking long-wave propagation in variable water depth. *Coastal Engineering*, 2025, 195, pp.104645. 10.1016/j.coastaleng.2024.104645 . hal-04768149

HAL Id: hal-04768149

<https://edf.hal.science/hal-04768149v1>

Submitted on 5 Nov 2024

HAL is a multi-disciplinary open access archive for the deposit and dissemination of scientific research documents, whether they are published or not. The documents may come from teaching and research institutions in France or abroad, or from public or private research centers.

L'archive ouverte pluridisciplinaire **HAL**, est destinée au dépôt et à la diffusion de documents scientifiques de niveau recherche, publiés ou non, émanant des établissements d'enseignement et de recherche français ou étrangers, des laboratoires publics ou privés.

A comparison of eight weakly dispersive Boussinesq-type models for non-breaking long-wave propagation in variable water depth

Guillaume Coulaud^{a,b,*}, Maria Teles^a and Michel Benoit^{a,b}

^aEDF R&D, Laboratoire National d'Hydraulique et Environnement (LNHE), 6 quai Watier, Chatou, 78400, France

^bLHSV, Saint-Venant Hydraulics Laboratory (Ecole des Ponts, EDF R&D), 6 quai Watier, Chatou, 78400, France

ARTICLE INFO

Keywords:

Boussinesq-type models

Dispersion

Nonlinearity

Linear shoaling

Trough instability

ABSTRACT

Weakly dispersive Boussinesq-type models are extensively used to model long-wave propagation in coastal areas and their interaction with coastal infrastructures. Many equations falling in this category have been formulated during the last decades, but few detailed comparisons between them can be found in the literature. In this work, we investigate theoretically and with computational experiments eight variants of the most popular models used by the coastal engineering community. Both weakly nonlinear and fully nonlinear models are considered, hoping to understand better when the additional complexity of the latter class of models is necessary or justified. We provide an overview and discuss the properties of these models, including the linear dispersion relation in uniform water depth, the second-order nonlinear coupling coefficient, the shoaling gradient, and the sensitivity to wave trough instabilities. The models are then numerically discretised using the same general strategy in a single numerical code, using fourth-order methods for time and space discretisation. Their capacity to simulate coastal wave propagation and their transformation when approaching the shore is assessed on three challenging one-dimensional benchmarks. It appears that fully nonlinear models are more consistent than their weakly nonlinear counterparts, which can occasionally perform better but show different behaviours depending on the case.

1. Introduction


Depth-averaged wave models have become very popular during the last decades since they have a relatively low computational cost compared to depth-resolving models while still achieving good accuracy in shallow- and possibly intermediate-water depths, typical of coastal wave propagation. Their applicability depends mainly on two non-dimensional parameters, quantifying nonlinear and dispersive effects arising during wave propagation: $\varepsilon = a/d$ for nonlinearity and $\mu = kd$ the relative water depth for dispersion, with a the local wave amplitude, d the local still water depth, $k = 2\pi/\lambda$ the local wavenumber, and λ the local wavelength. Dispersion is more significant for high values of μ , i.e. in deep waters or for short waves, while nonlinearity is typically more important in shallow waters or for high amplitude waves. Depth-averaged models are asymptotic models derived from the full Euler equations, usually within the shallow-water or long-wave framework, assuming $\mu^2 \ll 1$. The non-dimensional equations exhibit dispersive terms of order $\mathcal{O}(\mu^{2n})$, $n \in \mathbb{N}$. When terms of high order (high power in μ) are retained in the equations, the models can be applied to higher relative water depths μ , where dispersion is more important.

The NSWE derived by Barré de Saint-Venant (1871) are a powerful depth-integrated model to simulate wave propagation in shallow waters, in the surf zone where waves break and shorewards, where nonlinearity dominates. However, due to the hydrostatic pressure assumption, these equations

do not model frequency dispersion, no dispersive terms appear in the equations. They are thus not appropriate for intermediate and deep waters, where dispersive effects are important. The typical limit between shallow and intermediate depths is $\mu = \pi/10$ or $d/\lambda = 0.05$.

Boussinesq-type (BT) models are asymptotic depth-averaged dispersive wave models retaining the effects of dispersion of the lowest orders. They gained popularity in the late 1960s and extended the range of applicability of depth-integrated models to intermediate and potentially deep waters. They are essentially a shallow-water approximation to the fully dispersive and nonlinear water wave problem, with additional dispersive terms compared to the NSWE, arising when relaxing the hydrostatic pressure hypothesis. Many different BT models have been formulated, with dispersive and nonlinear terms of various orders. In this work, we are mainly interested in weakly dispersive BT models, including dispersive terms of the lowest order, i.e. $\mathcal{O}(\mu^2)$, with up to third-order spatial derivatives. At a given order in dispersion, BT models are further divided between weakly nonlinear and fully nonlinear models, depending on the assumptions made on the nonlinearity parameter ε . For weakly dispersive (in $\mathcal{O}(\mu^2)$) and weakly nonlinear models, one assumes that nonlinearity is small and of the same order as dispersion, i.e. $\varepsilon = \mathcal{O}(\mu^2)$, which leads to neglect all nonlinear dispersive terms which are of order $\mathcal{O}(\varepsilon\mu^2) = \mathcal{O}(\mu^4)$ or higher. For a fully nonlinear model, nonlinearity can be arbitrarily large, i.e. $\varepsilon = \mathcal{O}(1)$ and all nonlinear dispersive terms at the order of dispersion considered are kept. Fully nonlinear models should typically be able to describe more accurately nonlinear processes occurring during wave propagation, e.g. shoaling. Indeed, waves can reach values of ε higher than 1 when they are about to

*Corresponding author

 guillaume.coulaud@edf.fr (G. Coulaud); maria.teles@edf.fr (M. Teles); michel.benoit@edf.fr (M. Benoit)

ORCID(s): 0009-0001-0277-1269 (G. Coulaud); 0000-0001-7626-4625 (M. Teles); 0000-0003-4195-2983 (M. Benoit)

break; the weakly nonlinear hypothesis is thus not valid and fully nonlinear models should theoretically be more appropriate to model wave propagation and transformation up to the shoreline. This comes at the cost of increasing the complexity of the governing equations. The first weakly dispersive BT model can be attributed to Boussinesq (1872), valid for a horizontal bottom, and was extended by Mei and Le Méhauté (1966) to uneven bottoms (Dingemans, 1997). Peregrine (1967) also derived a weakly dispersive, weakly nonlinear model, often considered the original Boussinesq equations. These classical equations, however, are only applicable up to $\mu \approx 1.1$ in the intermediate-water range so that the celerity of the waves is accurately predicted. Various techniques have been used to improve the dispersive properties of BT models, such as using the velocity at a reference (possibly time-varying) elevation instead of the depth-averaged velocity (Nwogu, 1993), dividing the water column in more than one layer (Lynett and Liu, 2004; Chazel et al., 2009; Liu and Fang, 2016; Liu et al., 2018), or derive new equations, equivalent to the original ones at the order of dispersion considered, with one or several parameters which can be tuned to improve dispersion (Madsen and Sørensen, 1992; Madsen and Schäffer, 1998; Cienfuegos et al., 2006; Bonneton et al., 2011; Chazel et al., 2011). With these techniques, weakly dispersive BT models exhibit good dispersive properties up to deep-water conditions. High-order BT models, including terms of order $\mathcal{O}(\mu^4)$ or higher, have been formulated, further extending the range of applicability of depth-averaged models. Unfortunately, they are significantly more complex, with many more terms, including spatial derivatives of order up to five or more, which are difficult to handle numerically (Madsen et al., 1997a; Gobbi and Kirby, 1999; Madsen et al., 2003). Thus, most, if not all, operational codes are based on weakly dispersive models. Reviews on BT models can be found in Madsen and Schäffer (1999), Kirby (2003), Brocchini (2013) or Kirby (2016).

Other types of nearshore wave models exist. For example, Yang and Liu (2020) and Yang and Liu (2022) proposed new depth-integrated wave models, derived without making the long-wave assumption $\mu^2 \ll 1$. These models still have the advantage of reducing the dimension of the problem thanks to depth integration, while being applicable to study the propagation of more dispersive waves. This is achieved by making more or less complex assumptions on the vertical profile of the horizontal velocity. Although good accuracy in deeper waters comes at the cost of lengthy momentum equations, the highest order of mixed derivatives is three, as for weakly dispersive BT equations, making the discretisation of these equations easier than for high-order BT models. This work however focuses only on BT models.

Although many BT models have been derived in the literature, few comparisons have been made, and most of them compare only a limited number of models. Some comparisons of at least two BT models can be found in Wei et al. (1995), Gobbi and Kirby (1999), Kennedy et al. (2000), Kennedy et al. (2001), Kazolea and Delis (2013),

Filippini et al. (2015), Benoit et al. (2018), Kazolea and Ricchiuto (2018), Kazolea et al. (2019) or Lteif (2024). Kazolea and Ricchiuto (2024) recently thoroughly compared several BT models on many different cases. Additionally, in many comparisons, the various models show similar results, and in particular, fully nonlinear models do not seem to systematically have a clear upper hand over weakly nonlinear models despite their increased computational cost. In this work, we aim to compare some of the most popular weakly dispersive BT models in the literature, weakly and fully nonlinear, both theoretically and by simulating a few test cases. The goal is to put into evidence the advantages and/or limitations of the models considered.

The paper is organised as follows. In §2, the eight variants of BT models considered in this work are presented in their original form, as well as a reformulation enabling their numerical resolution. In §3, some theoretical analysis of the properties of the models is proposed through a second-order Stokes-type, a trough instability and a linear shoaling analysis. In §4, we briefly detail the numerical implementation of the models considered. In §5, the models are compared on three test cases of non-breaking long-wave propagation in variable water depth, and finally §6 provides a discussion of the results and a conclusion.

2. Boussinesq-type models considered

2.1. Generic formulations of BT equations

In this article, eight variants of weakly dispersive wave models are considered and compared. To make the presentation of the models lighter and easier, we restrict ourselves to one horizontal dimension (x axis) without loss of generality regarding their properties. Figure 1 is a sketch of the flow configuration with the main notations. The vertical axis points upwards, and its origin is located at the still water level (SWL). $h(x, t) = d(x) + \eta(x, t)$ is the total water depth, $\eta(x, t)$ the free-surface elevation, and $d(x)$ the still water depth. Since the equations are depth-averaged, there is a single representative velocity $u(x, t)$ at every position x . Depending on the model and the underlying assumptions made regarding the vertical variations of the horizontal velocity, this velocity can be either the depth-averaged horizontal velocity:

$$\bar{u}(x, t) = \frac{1}{h} \int_{-d}^{\eta} u(x, z, t) dz \quad (1)$$

or the horizontal velocity at a reference elevation in the water column denoted z_α , either fixed or variable in time:

$$u_\alpha(x, t) = u(x, z_\alpha, t). \quad (2)$$

All these models can be written in dimensional non-conservative form, called “form I” hereafter, expressing the conservation of mass and momentum, respectively:

$$h_t + (hu)_x = \mathcal{D}_h \quad (3)$$

$$u_t + \left(\frac{1}{2}u^2 + g\eta \right)_x = \mathcal{D}_u \quad (4)$$

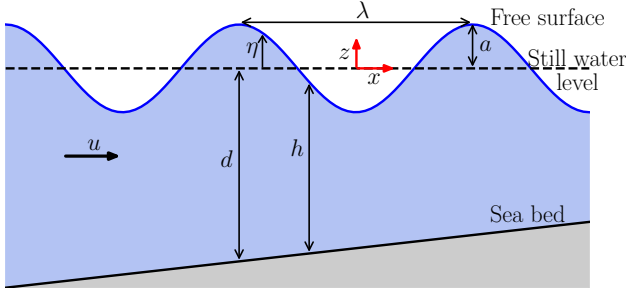


Figure 1: Flow configuration and notations. λ and a denote a characteristic wavelength and wave amplitude, respectively

The notation $(\cdot)_X$ denotes the partial derivative with respect to the variable X (x or t). $g = 9.81 \text{ m/s}^2$ is the acceleration of gravity. D_h and D_u are dispersive terms in $\mathcal{O}(\mu^2)$ since the models selected here are weakly dispersive. These terms are functions of h, u, η, d and their partial space and time derivatives, with at most third-order derivatives for the set of models considered here. D_h is different from zero only for models that do not use the depth-averaged velocity as the velocity variable. If $D_h = D_u = 0$ in Eqs. (3)–(4) and if $u = \bar{u}$, one recovers the non-dispersive NSW. E.

The dispersive term D_u includes mixed time and space derivatives of the velocity, which means the momentum equation (4) is implicit. To allow for the numerical resolution of the system, all momentum equations are reformulated here with an auxiliary variable $K = f(u, u_x, u_{xx}, h, h_x, \dots)$ which includes all terms where time derivatives appear. This solution strategy is quite common for solving BT models, see for instance Tonelli and Petti (2009); Roeber and Cheung (2012); Le Métayer et al. (2010); Shi et al. (2012).

With this auxiliary variable, the system (3)–(4) can be written under the equivalent form, called “form II”:

$$h_t + (hu)_x = D_h \quad (5)$$

$$K_t + \left(\frac{1}{2}u^2 + g\eta\right)_x = D_K \quad (6)$$

$$f(u, u_x, u_{xx}, d, d_x, h, h_x, \dots) = K \quad (7)$$

where now D_K does not include any time derivative. The equations (5)–(6) can then be integrated like any Ordinary Differential Equation (ODE), for instance with a Runge-Kutta (RK) method, and at each step, the elliptic equation (7) needs to be solved to recover the velocity u from the evolved variable K . In the following subsections, we give explicitly the two forms I and II of the variants of the models considered here.

2.2. Weakly nonlinear models

Weakly nonlinear models are derived assuming that waves are of finite but moderate amplitude, i.e. nonlinearity remains small. This means that $\mathcal{O}(\epsilon) = \mathcal{O}(\mu^2)$ and then nonlinear dispersive terms are of order at least $\mathcal{O}(\mu^4)$ and can be discarded. Three of the most popular weakly nonlinear models in the literature are considered: the models from Peregrine (1967), Madsen and Sørensen (1992) and Nwogu (1993).

2.2.1. Peregrine (1967)

The equations derived by Peregrine (1967) are the classical Boussinesq equations over variable bottoms. The equations are formulated with the depth-averaged velocity $u(x, t) = \bar{u}(x, t)$:

$$h_t + (h\bar{u})_x = 0 \quad (8)$$

$$\bar{u}_t + \left(\frac{1}{2}\bar{u}^2 + g\eta\right)_x = \frac{1}{2}d(d\bar{u})_{xxt} - \frac{1}{6}d^2\bar{u}_{xxt} \quad (9)$$

Reformulating the equations under form II, one gets:

$$D_h = 0 \quad (10)$$

$$D_K = 0 \quad (11)$$

$$K = \left(1 - \frac{1}{2}dd_{xx}\right)\bar{u} - dd_x\bar{u}_x - \frac{1}{3}d^2\bar{u}_{xx} \quad (12)$$

As the still water depth d and its spatial derivatives are known and constant in time, the matrix obtained after discretising the linear elliptic Eq. (12) is also constant. As pointed out in Kazolea and Ricchiuto (2024), this property is a direct consequence of the weak nonlinearity of the model.

2.2.2. Madsen and Sørensen (1992) (MS)

Madsen and Sørensen (1992) improved the model from Peregrine (1967) by applying a linear operator to include higher-order terms in the equations with a free parameter, denoted B hereafter, to enhance the dispersive properties. Their model also achieves excellent linear shoaling in its applicable range of relative water depth μ (see §3.4). The non-conservative form of the equations, formulated with the depth-averaged velocity $u(x, t) = \bar{u}(x, t)$, writes:

$$h_t + (h\bar{u})_x = 0 \quad (13)$$

$$\begin{aligned} \bar{u}_t + \left(\frac{1}{2}\bar{u}^2 + g\eta\right)_x &= \left(B + \frac{1}{3}\right)\frac{d^2}{h}(h\bar{u})_{xxt} \\ &+ Bg\frac{d^3}{h}\eta_{xxx} + \frac{d}{h}d_x\left(\frac{1}{3}(h\bar{u})_{xt} + 2Bg d\eta_{xx}\right) \end{aligned} \quad (14)$$

With $B = 1/15$, a Taylor expansion of the linear dispersion relation for $\mu \rightarrow 0$ matches that of the linear dispersion relation from Stokes theory up to fourth-order included (see §3.1). These equations have been used e.g. in Madsen et al. (1997b); Tonelli and Petti (2009); Kazolea and Delis (2013) or Kazolea and Ricchiuto (2024).

The form II of this model is:

$$D_h = 0 \quad (15)$$

$$\begin{aligned} D_K &= \left(B + \frac{1}{3}\right)\frac{d^2}{h^2}(h\bar{u})_x(h\bar{u})_{xx} + Bg\frac{d^3}{h}\eta_{xxx} \\ &+ \frac{dd_x}{h}\left(2Bg d\eta_{xx} - \frac{((h\bar{u})_x)^2}{3h}\right) \end{aligned} \quad (16)$$

$$\begin{aligned} K &= \left[1 - \left(B + \frac{1}{3}\right)\frac{d^2}{h}h_{xx} - \frac{dd_x}{3h}h_x\right]\bar{u} \\ &- \left[\left(B + \frac{1}{3}\right)\frac{2d^2h_x}{h} + \frac{dd_x}{3}\right]\bar{u}_x \\ &- \left(B + \frac{1}{3}\right)d^2\bar{u}_{xx} \end{aligned} \quad (17)$$

Unlike the Peregrine model, the coefficients of \bar{u} and its spatial derivatives in Eq. (17) vary in time here through the free surface elevation η appearing in the total water depth h . Note that if the momentum equation (14) is written in conservative form, then the matrix obtained from the discretisation of Eq. (17) is constant, as for Peregrine's model (see Tonelli and Petti (2009); Kazolea and Ricchiuto (2024) for example).

2.2.3. Nwogu (1993)

Nwogu (1993) derived a new set of Boussinesq equations by expanding the horizontal velocity as a second-order polynomial in z around the arbitrary elevation $z = z_\alpha$. The expansion writes:

$$u(z) = u_\alpha + u_2(z) \quad (18)$$

$$u_2(z) = \frac{1}{2} (z_\alpha^2 - z^2) u_{\alpha,xx} + (z_\alpha - z) (du_\alpha)_{xx} \quad (19)$$

with $u_\alpha = u(z = z_\alpha)$. This ansatz is accurate at $\mathcal{O}(\mu^2)$ in the long-wave framework. It comes from a Taylor expansion of the horizontal velocity along the vertical combined with the bed boundary and irrotationality conditions. The resulting equations, formulated with the velocity u_α are (dropping all nonlinear dispersive terms since the model is weakly nonlinear):

$$h_t + (hu_\alpha)_x = -\frac{\partial}{\partial x} \left[\left(\frac{1}{2} z_\alpha^2 - \frac{1}{6} d^2 \right) du_{\alpha,xx} + \left(z_\alpha + \frac{1}{2} d \right) d(du_\alpha)_{xx} \right] \quad (20)$$

$$u_{\alpha,t} + \left(\frac{1}{2} u_\alpha^2 + g\eta \right)_x = - \left[\frac{1}{2} z_\alpha^2 u_{\alpha,xx} + z_\alpha (du_{\alpha,t})_{xx} \right] \quad (21)$$

The reference elevation at which the velocity variable is considered is a fixed fraction of the still water depth, written $z_\alpha(x) = \zeta d(x)$, thus fixed in time. The coefficient $\zeta \in [-1, 0]$ is chosen so that the dispersion relation of the linearised equations best matches the exact dispersion relation from linear theory. As the MS model, this model has thus improved dispersive properties compared to the one from Peregrine (1967). More on that can be found in §3.1 where the linear dispersive properties of the models are compared. Nwogu (1993) found that when minimising the linear phase speed error over the shallow- and intermediate-water ranges ($0 < \mu < \pi$), the optimal coefficient is $\zeta \approx -0.531$. This BT model has been extensively used in numerical codes, among which BOUSS-2D (Nwogu and Demirebilek, 2001), BOSZ (Roeber and Cheung, 2012) or TUCWave (Kazolea et al., 2012; Kazolea and Delis, 2013; Kazolea et al., 2014).

The form II of this model writes:

$$D_h = -\frac{\partial}{\partial x} \left[\left(\frac{1}{2} z_\alpha^2 - \frac{1}{6} d^2 \right) du_{\alpha,xx} + \left(z_\alpha + \frac{1}{2} d \right) d(du_{\alpha,xx}) \right] \quad (22)$$

$$D_K = 0 \quad (23)$$

$$K = (1 + z_\alpha d_{xx}) u_\alpha + 2z_\alpha d_x u_{\alpha,x} + \left(\frac{1}{2} z_\alpha^2 + z_\alpha d \right) u_{\alpha,xx} \quad (24)$$

As for the Peregrine model, the coefficients of the velocity terms in Eq. (24) are constant in time, and the matrix corresponding to the linear operator linking K and u could be inverted once for all.

It should be noted that the mass conservation equation (20) is not exact. The exact conservation equation, obtained from depth-averaging the Euler continuity equation, is:

$$h_t + (h\bar{u})_x = 0 \quad (25)$$

Using the ansatz (18), the exact mass conservation equation (given the assumed velocity profile) would be:

$$h_t + \left(h (u_\alpha + \bar{u}_2) \right)_x = 0 \quad (26)$$

However, due to the assumption of weak nonlinearity, nonlinear dispersive terms in \bar{u}_2 are neglected and so D_h given by eq. (22) is not equal to $-(h\bar{u}_2)_x$, and mass is not conserved exactly.

2.3. Fully nonlinear models

Fully nonlinear models are derived without any particular assumption regarding nonlinearity, wave height can be arbitrarily high. These models are then theoretically more adapted to the simulation of wave propagation up to the coast since wave amplitude can increase due to shoaling up to the shoreline or the breaking point. Two families of fully nonlinear models are considered, the Serre-Green-Naghdi (SGN) equations (Serre, 1953; Green and Naghdi, 1976) and the model from Wei et al. (1995), as well as some of their improved versions.

2.3.1. Serre-Green-Naghdi (SGN) equations

The SGN equations were derived by Serre (1953) in one horizontal dimension for flat bottoms and by Su and Gardner (1969) and Green and Naghdi (1976) in two dimensions for arbitrary bottom topographies. They are the fully nonlinear extension of the weakly dispersive model from Peregrine (1967). Contrary to the previously mentioned BT models, this model also admits an exact energy conservation equation. The SGN equations have gained a lot of popularity in the last 15 years (see among many references Cienfuegos et al. (2006); Le Métayer et al. (2010); Bonneton et al. (2011); Dutykh et al. (2013); Panda et al. (2014); Lannes and Marche (2015); Filippini et al. (2016); Mitsotakis et al. (2017); Zoppou et al. (2017); Duran and Marche (2017); Pitt et al. (2021); Castro-Orgaz et al. (2022); Kazolea et al. (2023)). The equations, formulated with $u(x, t) = \bar{u}(x, t)$, are:

$$h_t + (h\bar{u})_x = 0 \quad (27)$$

$$\begin{aligned} \bar{u}_t + \left(\frac{1}{2} \bar{u}^2 + g\eta \right)_x &= \frac{1}{h} \frac{\partial}{\partial x} \left[\frac{1}{3} h^3 (\bar{u}_{xt} + \bar{u} \bar{u}_{xx} - \bar{u}_x^2) + \frac{1}{2} h^2 (\bar{u}_t d_x + \bar{u} (\bar{u} d_x)_x) \right] - d_x \left[\frac{1}{2} h (\bar{u}_{xt} + \bar{u} \bar{u}_{xx} - \bar{u}_x^2) + \bar{u}_t d_x + \bar{u} (\bar{u} d_x)_x \right] \end{aligned} \quad (28)$$

The form II of this model is:

$$\mathcal{D}_h = 0 \quad (29)$$

$$\mathcal{D}_K = \frac{\partial}{\partial x} \left[\bar{u}^2 \left(1 + \frac{1}{2} d_x^2 \right) - \bar{u}K \right. \\ \left. + \left(\frac{1}{2} h \bar{u}_x + d_x \bar{u} \right) h \bar{u}_x \right] \quad (30)$$

$$K = \left(1 - \eta_x d_x - \frac{1}{2} h d_{xx} \right) \bar{u} - h h_x \bar{u}_x - \frac{1}{3} h^2 \bar{u}_{xx} \quad (31)$$

2.3.2. Enhanced Serre-Green-Naghdi (eSGN) equations of Bonneton et al. (2011)

As shown in §3.1, the linear dispersive properties of the SGN equations are the same as those of Peregrine's model, and the theoretical limit of applicability of the equations falls in the intermediate-water range. Several attempts have been made to improve the model. For example, Cienfuegos et al. (2006) added higher-order terms to the equations following the approach of Madsen and Sørensen (1992), and, more recently, Clamond et al. (2017) derived an improved set of equations over horizontal beds by using a modified Lagrangian density. A popular set of enhanced SGN equations was derived by Bonneton et al. (2011). Their equations differ from the original SGN equations by terms of order $\mathcal{O}(\mu^4)$, they are thus equivalent at order $\mathcal{O}(\mu^2)$, and depend on a free constant parameter, denoted γ , used to enhance the dispersive properties. This model has a linear dispersion relation similar to those of the improved models previously described (see §3.1). The equations can be written (Li et al., 2019):

$$h_t + (h\bar{u})_x = 0 \quad (32)$$

$$\bar{u}_t + \left(\frac{1}{2} \bar{u}^2 + g\eta \right)_x = \frac{1}{h} \frac{\partial}{\partial x} \left\{ \frac{1}{3} h^3 \left[\gamma (\bar{u}_{xt} + \bar{u} \bar{u}_{xx}) \right. \right. \\ \left. \left. + (\gamma - 2) \bar{u}_x^2 + g(\gamma - 1) \eta_{xx} \right] + \frac{1}{2} h^2 \left[\gamma (\bar{u}_t d_x + \bar{u} \bar{u}_x d_x) \right. \right. \\ \left. \left. + \bar{u}^2 d_{xx} + g(\gamma - 1) \eta_x d_x \right] \right\} - d_x \left\{ \frac{1}{2} h \left[\gamma (\bar{u}_{xt} + \bar{u} \bar{u}_{xx}) \right. \right. \\ \left. \left. + (\gamma - 2) \bar{u}_x^2 + g(\gamma - 1) \eta_{xx} \right] + \gamma (\bar{u}_t d_x + \bar{u} \bar{u}_x d_x) \right. \\ \left. + \bar{u}^2 d_{xx} + g(\gamma - 1) \eta_x d_x \right\} \quad (33)$$

In order to optimise the linear phase and group speeds for $\mu < 4$ in the deep-water range, the suggested value of γ in Bonneton et al. (2011) is $\gamma = 1.159$. If $\gamma = 1$, one recovers the original SGN equations (27)–(28).

The form II of the model written in conservative form was derived by Li et al. (2019). Here, we derived the form II of the non-conservative version of the model and obtained:

$$\mathcal{D}_h = 0 \quad (34)$$

$$\mathcal{D}_K = \frac{\partial}{\partial x} \left\{ \bar{u}^2 \left(1 + \frac{1}{2} \gamma d_x^2 \right) - \bar{u}K \right. \\ \left. + \left[\left(\frac{7}{6} \gamma - \frac{2}{3} \right) h \bar{u}_x + \gamma d_x \bar{u} \right] h \bar{u}_x \right. \\ \left. - \frac{1}{2} (\gamma - 1) h \bar{u}^2 d_{xx} \right. \\ \left. + (\gamma - 1) g \left(\frac{1}{3} h^2 \eta_{xx} + h \eta_x d_x \right) \right\} \\ + (\gamma - 1) \left[\frac{1}{3} h \bar{u}_x^2 (2\eta_x - d_x) \right. \\ \left. + \frac{1}{2} \bar{u}^2 (d_x - \eta_x) d_{xx} \right] \\ + (\gamma - 1) g \left[\frac{1}{3} h \eta_{xx} (\eta_x - 2d_x) \right. \\ \left. - \eta_x \left(\frac{1}{2} h d_{xx} + d_x^2 \right) \right] \\ K = \left(1 - \gamma \eta_x d_x - \frac{1}{2} \gamma h d_{xx} \right) \bar{u} - \gamma h h_x \bar{u}_x \\ - \frac{1}{3} \gamma h^2 \bar{u}_{xx} \quad (35)$$

2.3.3. Wei et al. (1995) (WKGS)

In deriving his model, Nwogu (1993) neglected nonlinear dispersive terms. These terms are included in the model from Wei et al. (1995), hereafter abbreviated as WKGS. The model can be derived following Nwogu's approach, expanding the horizontal velocity as a second-order polynomial in z around its value at an arbitrary elevation $z_\alpha = \zeta d$, and retaining all terms. As in Nwogu (1993), WKGS considered $\zeta = -0.531$ to optimise the linear phase speed of the model. The resulting governing equations formulated with $u = u_\alpha$ are:

$$h_t + (h u_\alpha)_x = - \frac{\partial}{\partial x} \left\{ h \left[\left(\frac{1}{2} z_\alpha^2 - \frac{1}{6} (d^2 - d\eta) \right. \right. \right. \\ \left. \left. + \eta^2 \right) u_{\alpha,xx} + \left(z_\alpha + \frac{1}{2} (d - \eta) \right) (d u_\alpha)_{xx} \right] \right\} \\ u_{\alpha,t} + \left(\frac{1}{2} u_\alpha^2 + g\eta \right)_x = - \left[\frac{1}{2} z_\alpha^2 u_{\alpha,xx} + z_\alpha (d u_\alpha)_{xx} \right] \\ + \frac{\partial}{\partial x} \left[\frac{1}{2} \eta^2 u_{\alpha,xt} + \eta (d u_\alpha)_x - (z_\alpha - \eta) u_\alpha (d u_\alpha)_{xx} \right. \\ \left. - \frac{1}{2} (z_\alpha^2 - \eta^2) u_\alpha u_{\alpha,xx} - \frac{1}{2} ((d u_\alpha)_x + \eta u_{\alpha,x})^2 \right] \quad (37)$$

This fully nonlinear BT model is notably more complicated than Nwogu's, with several additional gradient operations and mixed space-time derivatives. Reformulated under form II, this model writes:

$$\mathcal{D}_h = - \frac{\partial}{\partial x} \left\{ h \left[\left(\frac{1}{2} z_\alpha^2 - \frac{1}{6} (d^2 - d\eta + \eta^2) \right) u_{\alpha,xx} \right. \right. \\ \left. \left. + \left(z_\alpha + \frac{1}{2} (d - \eta) \right) (d u_\alpha)_{xx} \right] \right\} \quad (39)$$

$$\mathcal{D}_K = - \frac{\partial}{\partial x} \left[\frac{1}{2} (d_x u_\alpha + h u_{\alpha,x})^2 + h_t (d_x u_\alpha + h u_{\alpha,x}) \right. \\ \left. + u_\alpha (z_\alpha - \eta) \left(\frac{1}{2} (z_\alpha + \eta) u_{\alpha,xx} + (d u_\alpha)_{xx} \right) \right] \quad (40)$$

$$\begin{aligned}
K = & (1 + (z_\alpha - \eta)d_{xx} - \eta_x d_x) u_\alpha \\
& + (2(z_\alpha - \eta)d_x - \eta_x h) u_{\alpha,x} \\
& + \left(\frac{1}{2} z_\alpha^2 + z_\alpha d - \eta \left(d + \frac{1}{2} \eta \right) \right) u_{\alpha,xx}
\end{aligned} \quad (41)$$

The term h_t in Eq. (40) is computed from the continuity equation (37), i.e. $h_t = -(hu)_x + D_h$, so that there is no time derivative in the final expression of Eq. (40).

Contrary to Nwogu's model, this model conserves mass exactly. The model being fully nonlinear, no dispersive term is neglected when depth-integrating the Euler continuity equation and so eq. (39) can also be written $D_h = -(h\bar{u}_2)_x$, with u_2 defined in eq. (19), which means the mass conservation equation (37) is:

$$h_t + (h(u_\alpha + \bar{u}_2))_x = 0 \quad (42)$$

which is the exact mass conservation equation (25).

2.3.4. Kennedy et al. (2001) (KKCD)

Kennedy et al. (2001), hereafter abbreviated as KKCD, improved the nonlinear properties of the WKGS model by allowing the elevation z_α to vary in time. They assumed $z_\alpha(x, t) = \zeta d(x) + \beta \eta(x, t)$, with the constant parameters ζ and β chosen to improve nonlinear properties and the linear dispersion relation. With this definition of z_α the mass conservation equation (37) of WKGS is unchanged, and the only difference with Eq. (38) is that the first term on the right-hand side (RHS):

$$-\left[\frac{1}{2} z_\alpha^2 u_{\alpha,xx} + z_\alpha (du_{\alpha,t})_{xx} \right] \quad (43)$$

now becomes:

$$-\frac{\partial}{\partial t} \left[\frac{1}{2} z_\alpha^2 u_{\alpha,xx} + z_\alpha (du_\alpha)_{xx} \right] \quad (44)$$

Choosing $\zeta \approx -0.553$ optimises the asymptotic linear dispersion relation, and $\beta \approx 0.19$ optimises the nonlinear properties of the equations (more details in §3). This set of parameters designates the ‘‘optimal KKCD’’ (oKKCD) model.

Another set of parameters is interesting. If one chooses $\beta = \zeta + 1$, then $z_\alpha(x, t) = -d(x) + \beta h(x, t)$, i.e. the reference elevation is a fixed fraction of the total water column. With this choice, all terms in the equations depend on h or derivatives of d and η , but not d directly, thus they do not depend on the definition of the SWL. These equations are the ‘‘datum-invariant KKCD’’ (diKKCD) model and are the basis of the well-known software FUNWAVE-TVD (Shi et al., 2012). $\zeta \approx -0.553$ is also chosen here, and so $\beta \approx 0.447$. The resulting Form I of the equations is:

$$\begin{aligned}
h_t + (hu_\alpha)_x = & -\frac{\partial}{\partial x} \left[\frac{1}{2} h^3 \left(\beta^2 - \frac{1}{3} \right) u_{\alpha,xx} \right. \\
& \left. + h^2 \left(\beta - \frac{1}{2} \right) (d_x u_{\alpha,x} + (d_x u_\alpha)_x) \right]
\end{aligned} \quad (45)$$

$$\begin{aligned}
u_{\alpha,t} + \left(\frac{1}{2} u_\alpha^2 + g\eta \right)_x = & -\frac{\partial}{\partial x} \left[\frac{1}{2} (\beta^2 - 1) h^2 u_\alpha u_{\alpha,xx} \right. \\
& \left. + \frac{1}{2} (hu_{\alpha,x} + d_x u_\alpha)^2 + (\beta - 1) hu_\alpha (d_x u_{\alpha,x} + (d_x u_\alpha)_x) \right] \\
& - \left[\frac{1}{2} (\beta^2 - 1) h^2 u_{\alpha,xx} - h\eta_x u_{\alpha,xt} - \eta_x d_x u_{\alpha,t} \right. \\
& \left. + (\beta - 1) h (d_x u_{\alpha,xt} + (d_x u_{\alpha,t})_x) \right. \\
& \left. + \beta h_t (\beta h u_{\alpha,xx} + d_x u_{\alpha,x} + (d_x u_\alpha)_x) \right]
\end{aligned} \quad (46)$$

Kennedy et al. (2001) noticed that, among the different possibilities, the diKKCD is more stable than the oKKCD, both being more stable than the original WKGS for which z_α has no time dependency. This property is particularly interesting since it has been demonstrated in Madsen and Fuhrman (2020) and Kirby (2020) that WKGS (among other fully nonlinear models) is subject to instabilities occurring in wave troughs for sufficiently high Nyquist wavenumbers, i.e. fine spatial discretisations. As will be shown in §3.3, the oKKCD model is also subject to this instability but for a reduced range of relative water depths μ and trough elevations. In contrast, the diKKCD model is free from such instability.

The form II of the model is the same as WKGS, given by Eqs. (39)–(41), the only difference being the expression of the now time-varying reference elevation z_α . The model being fully nonlinear, it conserves mass correctly as does the WKGS model.

3. Theoretical comparison of the properties of the models

This section presents an analytical comparison of some of the properties of the models. We perform a second-order Stokes-type analysis of the models presented earlier and a trough instability analysis following Madsen and Fuhrman (2020). Finally, we present a linear shoaling analysis, as was done in Madsen and Schäffer (1998) for example. The models' performances, when used to simulate wave propagation, will be discussed in §5.

3.1. Linear dispersive properties

Until further notice, we consider a horizontal bottom (d is constant). We make a perturbation expansion and look for second-order solutions to the equations as plane progressive regular waves of the form:

$$\eta = a_1 \cos(kx - \omega t) + \varepsilon a_2 \cos(2(kx - \omega t)) \quad (47)$$

$$u = u_1 \cos(kx - \omega t) + \varepsilon u_2 \cos(2(kx - \omega t)) \quad (48)$$

with $\varepsilon \ll 1$ and ω the angular frequency. These expressions are inserted in the governing equations. At first order (terms in $\mathcal{O}(1)$), we get the linear dispersion relation $C = \omega/k$. Then, looking at terms in $\mathcal{O}(\varepsilon)$, we get the amplitude of the second-order bound harmonic, a_2 .

Since the initial goal of BT models is to take dispersion into account to be applicable in deeper waters than the NSWE, we first look at the linear dispersion relation

Model	Coefficient σ
Nwogu, WKGS, oKKCD, diKKCD	$-\left(\alpha + \frac{1}{3}\right)$ with $\alpha = \frac{1}{2}\zeta^2 + \zeta$
MS	B
eSGN	$\frac{1}{3}(\gamma - 1)$

Table 1

Coefficient σ appearing in Eq. (51) for the models. ζ , B and γ are defined in §2.

obtained with the models. The exact phase speed obtained from linear theory is, together with the first terms of its Taylor expansion for small values of $\mu = kd$:

$$\frac{C_e^2}{gd} = \frac{\tanh \mu}{\mu} = 1 - \frac{1}{3}\mu^2 + \frac{2}{15}\mu^4 + \mathcal{O}(\mu^6) \quad (49)$$

The linear phase speed is the same for the Peregrine and SGN models and is denoted C_1 . The general expression of the linear phase speed is the same for all the improved models considered here, namely the Nwogu, MS, eSGN, WKGS and both variants of KKCD models, and is denoted C_2 . Their expressions are (again with the first terms of their Taylor expansions):

$$\frac{C_1^2}{gd} = \frac{1}{1 + \frac{1}{3}\mu^2} = 1 - \frac{1}{3}\mu^2 + \frac{1}{9}\mu^4 + \mathcal{O}(\mu^6) \quad (50)$$

$$\begin{aligned} \frac{C_2^2}{gd} &= \frac{1 + \sigma\mu^2}{1 + \left(\sigma + \frac{1}{3}\right)\mu^2} \\ &= 1 - \frac{1}{3}\mu^2 + \frac{1}{3}\left(\sigma + \frac{1}{3}\right)\mu^4 + \mathcal{O}(\mu^6) \end{aligned} \quad (51)$$

The expression of the coefficient σ depends on the model and is given in table 1. Compared with Eq. (50), σ introduces a degree of freedom in Eq. (51) to improve the dispersion relation of the second family of models.

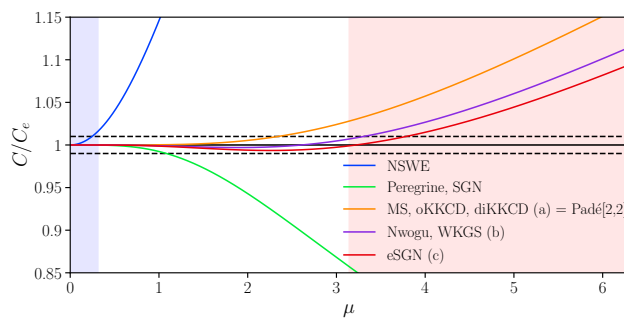


Figure 2: Ratio of the linear phase speed to the theoretical one for the different models. The blue and red areas represent the shallow- and deep-water ranges, respectively.

The ratio of the linear phase speed of the BT models to the one given by linear theory Eq. (49) against $\mu = kd$ is

plotted in figure 2. The horizontal dashed lines mark the 1% relative error limits. For reference, the linear phase speed predicted by the NSWSE is included in the plot. It is $C = \sqrt{gd}$ and is independent of the wavelength since the equations are non-dispersive. As one can see, the classical BT model from Peregrine and the SGN equations, i.e. C_1 in Eq. (50) (light green curve), only exhibit accurate dispersive properties in shallow waters and at the beginning of the intermediate-water range, roughly up to $\mu = 1.2$.

For C_2 in Eq. (51), several options are possible for choosing the free parameter. For each model, the linear dispersion relation plotted in figure 2 is the one with the parameter choices made in the references where the model was derived. These choices were recalled in §2 where the models were presented. We present these choices here, bearing in mind that any particular value of σ in Eq. (51) could be reached by all the models MS, Nwogu, WKGS, oKKCD, diKKCD and eSGN using the relations of table 1.

A first choice is to match the Padé[2,2] approximation of Eq. (49), namely:

$$\frac{C^2}{gd} \approx \frac{1 + \frac{1}{15}\mu^2}{1 + \frac{2}{5}\mu^2} \quad (52)$$

or, equivalently, to match the coefficient of the μ^4 term in the Taylor expansion of Eq. (49). This choice, called choice (a) hereafter, was made by Madsen and Sørensen (1992) and Kennedy et al. (2001) and leads to $\sigma = 1/15 \approx 0.0667$, and consequently to $B = 1/15$ for the MS model, and $\alpha = -2/5$ ($\zeta \approx -0.553$) for the oKKCD and diKKCD models. The same dispersion relation could be obtained with $\gamma = 6/5 = 1.2$ for the eSGN model. The corresponding curve is plotted in orange in figure 2. A clear improvement in comparison to the Peregrine-SGN relation (Eq. (50)) can indeed be observed in the range of intermediate water depth $kd \in [0.5, 2.4]$, but the error then increases rapidly for higher values of kd .

Another widely used option is to select the value of σ which optimises the linear phase speed and/or group speed over a range of kd , typically taken as $[0, kd_{max}]$. Various values of kd_{max} could be considered. We show here two examples. The first one (called choice (b)), due to Nwogu (1993) and also considered by Wei et al. (1995), is to minimise the phase speed error up to $kd_{max} = \pi$ and leads to $\zeta = -0.531$ ($\alpha = -0.39$, and $\sigma \approx 0.057$, a value lower than the one of choice (a)). This corresponds to the purple curve in figure 2. As another example, Bonneton et al. (2011) chose $kd_{max} = 4$ and optimised the normalised error on the phase and group speeds and obtained $\gamma = 1.159$ for the eSGN model (choice (c), red curve in figure 2), corresponding to $\sigma = 0.053$, again lower than the value of choice (b). The Nwogu, WKGS and KKCD models with choice (b) and the eSGN equations with choice (c) show less than 1% error up to the deep-water range, with slightly larger error over the range $kd \in [0.7, 1.8]$ in comparison with the choice (a) though. We again stress that the MS, Nwogu, WKGS and KKCD models could all achieve the same linear dispersion

relation as the one shown here for the eSGN with choice (c) by choosing their free parameter to reach the same value of σ .

3.2. Second-order bound wave amplitude

By looking at terms in $O(\varepsilon)$ in Eqs. (47)-(48), and solving a linear system of equations, one gets the amplitude of the second-order bound wave, a_2 , expressed in non-dimensional form as a_2/a_1 :

Weakly nonlinear models:

- Peregrine:

$$\frac{a_2}{a_1} = \frac{3ka_1}{4\mu^3} \left(1 + \frac{8}{9}\mu^2\right) \quad (53)$$

- MS:

$$\frac{a_2}{a_1} = \frac{3ka_1}{4\mu^3} \left(1 + \left(B + \frac{1}{9}\right)\mu^2\right) \quad (54)$$

- Nwogu:

$$\frac{a_2}{a_1} = \frac{3ka_1}{4\mu^3} \frac{1 - \frac{14}{3}\left(\alpha + \frac{1}{7}\right)\mu^2 + \frac{8}{3}\alpha\left(\alpha + \frac{1}{3}\right)\mu^4}{1 - \left(\alpha + \frac{1}{3}\right)\mu^2} \quad (55)$$

Fully nonlinear models:

- SGN:

$$\frac{a_2}{a_1} = \frac{3ka_1}{4\mu^3} \left(1 + \frac{1}{3}\mu^2\right) \quad (56)$$

- eSGN:

$$\frac{a_2}{a_1} = \frac{3ka_1}{4\mu^3} \left(1 + \frac{5}{3}\left(\gamma - \frac{4}{5}\right)\mu^2 + \frac{4}{9}(\gamma - 1)\left(\gamma - \frac{1}{3}\right)\mu^4\right) \quad (57)$$

- WKGS:

$$\frac{a_2}{a_1} = \frac{3ka_1}{4\mu^3} \left[1 - 6\left(\alpha + \frac{5}{18}\right)\mu^2 + \frac{26}{3}\left(\alpha^2 + \frac{10}{13}\alpha + \frac{7}{39}\right)\mu^4 - \frac{8}{3}\left(\alpha + \frac{1}{3}\right)\left(\alpha^2 + \alpha + \frac{1}{3}\right)\mu^6\right] / \left[1 - \left(\alpha + \frac{1}{3}\right)\mu^2\right] \quad (58)$$

- oKKCD:

$$\frac{a_2}{a_1} = \frac{3ka_1}{4\mu^3} \left[1 - 6\left(\alpha + \frac{5}{18}\right)\mu^2 + \frac{26}{3}\left(\alpha^2 + \frac{10}{13}\alpha - \frac{4}{39}\xi\right) + \frac{7}{39}\mu^4 - \frac{8}{3}\left(\alpha + \frac{1}{3}\right)\left(\alpha^2 + \alpha - \frac{1}{3}\xi + \frac{1}{3}\right)\mu^6\right] / \left[1 - \left(\alpha + \frac{1}{3}\right)\mu^2\right] \quad (59)$$

Model	c_2	c_4
Peregrine	$\frac{8}{9}$	0
MS	$B + \frac{1}{9}$	0
Nwogu	$-\frac{1}{3}(1 + 11\alpha)$	0
WKGS	$-\frac{1}{3}(4 + 15\alpha)$	$\frac{11}{3}\alpha(\alpha + 1) + \frac{10}{9}$
oKKCD	$-\frac{1}{3}(4 + 15\alpha)$	$\frac{11}{3}\alpha(\alpha + 1) + \frac{10}{9} - \frac{8}{9}\xi$
diKKCD	$-\frac{1}{3}(4 + 15\alpha)$	$\frac{11}{3}\alpha^2 + \frac{17}{9}\alpha + \frac{2}{9}$
SGN	$\frac{1}{3}$	0
eSGN	$\frac{5}{3}\left(\gamma - \frac{4}{5}\right)$	$\frac{4}{9}\left(\gamma - \frac{1}{3}\right)(\gamma - 1)$

Table 2

Coefficients c_2 and c_4 appearing in equation (61) for the eight BT models. ζ , B and γ are defined in §2.

- diKKCD:

$$\frac{a_2}{a_1} = \frac{3ka_1}{4\mu^3} \left[1 - 6\left(\alpha + \frac{5}{18}\right)\mu^2 + \frac{26}{3}\left(\alpha^2 + \frac{22}{39}\alpha + \frac{1}{13}\right)\mu^4 - \frac{8}{3}\alpha\left(\alpha + \frac{1}{3}\right)^2\mu^6\right] / \left[1 - \left(\alpha + \frac{1}{3}\right)\mu^2\right] \quad (60)$$

In all these expressions, a_2/a_1 is proportional to the Ursell number ka_1/μ^3 , i.e. the ratio of wave steepness ka_1 to dispersion parameter μ (to the power of 3). ξ in Eq. (59) is defined as $\xi = \beta(1 + \zeta)$. For diKKCD $\beta = 1 + \zeta$, so that $\xi = 1 + 2\alpha$. Putting this expression in Eq. (59) gives Eq. (60).

Making a Taylor expansion for $\mu \rightarrow 0$, one gets the following generic approximation for a_2/a_1 for each model:

$$\frac{a_2}{a_1} = \frac{3ka_1}{4\mu^3} \left(1 + c_2\mu^2 + c_4\mu^4 + O(\mu^6)\right) \quad (61)$$

with the c_2 and c_4 coefficients depending on the model, given in table 2. The exact expression for the second-order amplitude from Stokes' theory is:

$$\begin{aligned} \frac{a_{2e}}{a_1} &= \frac{ka_1}{4} \coth(\mu) (3 \coth^2(\mu) - 1) \\ &= \frac{3ka_1}{4\mu^3} \left(1 + \frac{2}{3}\mu^2 + \frac{7}{45}\mu^4 + O(\mu^6)\right) \end{aligned} \quad (62)$$

For c_2 to match the coefficient $2/3$ in the expansion of a_{2e} , the value of α must be $-3/11 \approx -0.27$ for Nwogu's model and $-2/5$ for the variants of the KKCD and the WKGS models (corresponding to $\zeta \approx -0.553$, choice (a) from the previous section). For the former, this value leads to a poor prediction of the linear phase speed; meanwhile,

the agreement on the linear dispersion relation is also good for the latter. This proves that the additional nonlinear terms in WKGS and KKCD theoretically allow a more accurate description of the nonlinear properties. For oKKCD and $\alpha = -2/5$, $c_4 = 52/225 - 8\xi/9$. Choosing $\xi = 17/200$ (i.e. $\beta \approx 0.19$), c_4 matches the $O(\mu^4)$ coefficient $7/45$.

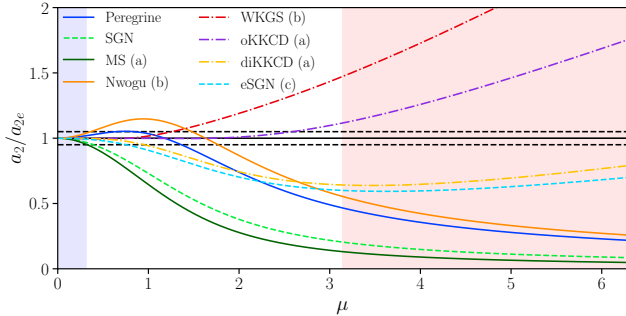


Figure 3: Ratio of the second-order correction of the free surface to the exact one for the different models. The blue and red areas represent the shallow- and deep-water ranges, respectively.

Figure 3 represents the variations of the ratio a_2/a_{2e} with μ for the eight variants of the models. The horizontal dashed lines mark the $\pm 5\%$ error range. The models from Peregrine and Nwogu show similar trends, first overestimating then underestimating wave amplitude for increasing μ , and the former being closer to the theory for $\mu < 1.5$. As a fully nonlinear model, WKGS performs better than Nwogu's model for approximately $\mu < 1.5$. However, both models show significant errors for higher relative water depths, respectively overestimating and underestimating the second-order wave amplitude. In particular, the WKGS model predicts excessive second-order amplitude with increasing μ : the overestimation reaches 50% at $\mu \approx \pi$, and 100% at $\mu \approx 4.8$.

The oKKCD model performs much better than WKGS: it shows an acceptable accuracy up to the deep-water limit but tends to overestimate a_2 as μ increases in the deep water range (in a notably less marked manner compared to WKGS, though). On the contrary, the diKKCD model underestimates the second-order amplitude by -36% at most for $\mu \in [0, 2\pi]$. The MS and the SGN models show the largest errors, both considerably underestimating the amplitude in the intermediate-water range and beyond. The eSGN equations are comparable to the diKKCD model.

Overall, BT models have much better linear dispersive properties compared to their weakly nonlinear properties. Only the oKKCD model exhibits both good dispersive and nonlinear properties over the shallow and intermediate depth ranges. Although this analysis is valid only for small waves, some of the conclusions drawn here have also been reported by other researchers when studying the propagation of nonlinear waves, namely that the Nwogu and Peregrine models tend to overestimate wave height in some situations (here at the beginning of the intermediate-water range), or that the MS model and the SGN equations tend to underestimate

it (see e.g. Kennedy et al. (2000), Filippini et al. (2015) or Kazolea and Ricchiuto (2024)).

3.3. Trough instabilities

Recently, Madsen and Fuhrman (2020) and Kirby (2020) unveiled a nonlinear instability mechanism affecting some BT models for sufficiently deep wave troughs and high relative water depths. These are called "trough instabilities", and this mechanism only affects fully nonlinear models. Many well-known models were found to be prone to these instabilities in Madsen and Fuhrman (2020) and Kirby (2020). Among the BT models considered here, these two references show that the WKGS model is prone to this instability, while the SGN and weakly nonlinear ones are not.

Here, we investigate the model variants not covered in these two references, namely the eSGN equations from Bonneton et al. (2011) and the extended WKGS models (oKKCD and diKKCD) from Kennedy et al. (2001), to determine whether trough instabilities can arise when solving these equations. To do so, we follow the procedure detailed in §3.4 in Madsen and Fuhrman (2020), and look for small amplitude harmonic solutions to the equations, with a mean water level below the SWL. This corresponds to perturbations on top of the trough of a wave train. We still consider a horizontal bottom. The ansatz for free surface elevation and horizontal velocity is:

$$\eta = \delta d + \varepsilon A_0 \cos(kx - \omega t) \quad (63)$$

$$u = \varepsilon B_0 \cos(kx - \omega t) \quad (64)$$

with $\delta \in [-1, 0]$ and $\varepsilon \ll 1$. We insert this ansatz in the governing equations and collect the $\mathcal{O}(\varepsilon)$ terms to determine the dispersion relation, which can have singularities for specific values of δ . If ω^2/k^2 can take negative values for some couples (δ, μ) , then the model is affected by trough instabilities.

For the eSGN equations, one gets:

$$\frac{\omega^2}{k^2 g d} = (\delta + 1) \frac{1 + \frac{1}{3}(\gamma - 1)(\delta + 1)^2 \mu^2}{1 + \frac{1}{3}\gamma(\delta + 1)^2 \mu^2} \quad (65)$$

which is always strictly positive for the values of γ considered, i.e. 1 (SGN) and 1.159 (eSGN).

For the model from Kennedy et al. (2001), we get:

$$\begin{aligned} \frac{\omega^2}{k^2 g d} = (\delta + 1) & \left\{ 1 - \mu^2 \left[\alpha + \frac{1}{3} + \left(\xi - \frac{1}{3} \right) \delta \right. \right. \\ & \left. \left. + \left(\frac{1}{4} \xi^2 / \left(\alpha + \frac{1}{2} \right) - \frac{1}{6} \right) \delta^2 \right] \right\} / \left\{ 1 - \mu^2 \left[\alpha \right. \right. \\ & \left. \left. + (\xi - 1) \delta + \left(\frac{1}{4} \xi^2 / \left(\alpha + \frac{1}{2} \right) - \frac{1}{2} \right) \delta^2 \right] \right\} \end{aligned} \quad (66)$$

For WKGS (with $\alpha = -2/5$, $\xi = 0$) and oKKCD ($\alpha = -2/5$, $\xi = 17/200$), the phase speed has a singularity at a given relative depth μ for sufficiently low values of δ . For diKKCD, $\xi = 1 + 2\alpha$ and the dispersion relation becomes:

$$\frac{\omega^2}{k^2 g d} = (\delta + 1) \frac{1 - \left(\alpha + \frac{1}{3} \right) (\delta + 1)^2 \mu^2}{1 - \alpha (\delta + 1)^2 \mu^2} \quad (67)$$

which no longer has singularities since $1 - \alpha(\delta + 1)^2\mu^2$ is always strictly positive. Furthermore, diKKCD is not subject to trough instabilities provided that $\alpha < -1/3$, which is the case for values giving accurate linear dispersion (choices (a) and (b) mentioned in §3.1). For WKGS and oKKCD, the results of the stability analysis, following the procedure from Madsen and Fuhrman (2020), are shown in figure 4. The solid blue and red lines represent the couples (δ, μ) for which the dispersion relation is singular, and the hatched areas are the zones of instability. A computation will be unstable if δ has a sufficiently small value, i.e. if the trough is deep enough, and if some of the resolved wavenumbers μ fall in the unstable range. To avoid instabilities, the Nyquist wavenumber $\pi/\Delta x$ must be low enough so that all resolved wavenumbers are stable. Lower values of δ and higher values of μ are needed for oKKCD than WKGS to fall in the unstable zone. Thus, the optimised model is less subject to trough instabilities than the original WKGS model, while the diKKCD model with classical parameter choices is free from such instabilities. This is in line with the findings from Kennedy et al. (2001) mentioned in §2 regarding the stability of the WKGS and KKCD equations.

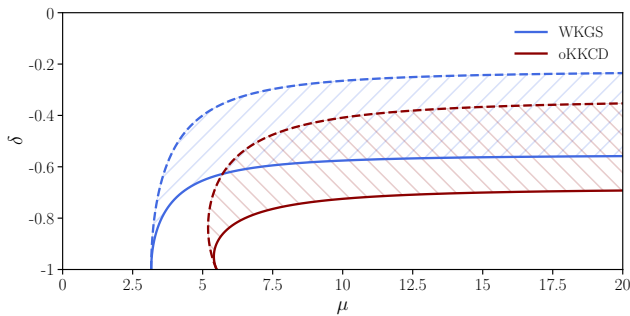


Figure 4: Zones of trough instabilities for the WKGS and oKKCD model. The solid lines represent the singularities of the linear phase speed, and the hatched areas between the solid lines and the dashed lines are the theoretical zones of trough instability.

A common feature of the eSGN and the diKKCD equations is that they do not depend on the still water depth d but only its spatial derivatives. In WKGS and oKKCD, however, some dispersive terms depend on the definition of the SWL. We examined all the models that were found to suffer from trough instabilities in Madsen and Fuhrman (2020), namely the models from Wei et al. (1995), Madsen and Schäffer (1998), Agnon et al. (1999), Gobbi et al. (2000), Madsen et al. (2002), Lynett and Liu (2004), and Liu et al. (2018). It appears that they all also depend on the definition of the SWL. The explanation behind the presence or absence of trough instabilities in a given model has yet to be found, but based on these observations, the authors believe it has to do with the dependence of the equations on the SWL definition, although this remains to be proven.

3.4. Linear shoaling gradient

Finally, we compare the linear shoaling properties of the models. The bottom is no longer assumed to be horizontal. In the linear regime and for mildly varying bottoms, the linear shoaling gradient S is defined such that:

$$\frac{A_x}{A} = -S \frac{d_x}{d} \quad (68)$$

with $A(x)$ the local wave amplitude, and $d(x)$ the local still water depth. The shoaling gradient predicted by linear theory was derived by Madsen and Sørensen (1992), and its expression is:

$$S_e = 2\mu \frac{\sinh(2\mu) + \mu(1 - \cosh(2\mu))}{(2\mu + \sinh(2\mu))^2} \quad (69)$$

Following Madsen and Schäffer (1998), we linearise the model's equations assuming η and u are small and look for solutions of the form:

$$\eta(x, t) = A(x) \exp(i(\psi(x) - \omega t)) \quad (70)$$

$$u(x, t) = D(x) (1 + i\sigma(x)d_x) \exp(i(\psi(x) - \omega t)) \quad (71)$$

with ψ such that $d\psi/dx = k(x)$ the local wavenumber. The term $i\sigma d_x$ allows a phase shift between u and η . Assuming a mildly varying bottom, d , k , A , D , and σ are slowly varying functions of the position x , and so all their space derivatives of order higher than one, as well as products of derivatives, will be neglected. With these assumptions, one obtains the equation:

$$s_1 \frac{A_x}{A} + s_2 \frac{k_x}{k} + s_3 \frac{d_x}{d} = 0 \quad (72)$$

Differentiating the dispersion relation with respect to x gives:

$$\frac{k_x}{k} = -\frac{s_5 d_x}{s_4 d} \quad (73)$$

and the linear shoaling gradient can be obtained as:

$$S = \frac{s_3 - s_2 s_5 / s_4}{s_1} \quad (74)$$

The expressions for the linear shoaling gradient for the Peregrine and eSGN models can be found in Filippini (2016), while Madsen and Sørensen (1992) derived the expression for their model. Finally, the expression for Nwogu's model and its fully nonlinear extensions can be found in Lee et al. (2003). These expressions are recalled here for completeness. The linear shoaling gradient for the SGN equations and Peregrine's model writes:

$$S = \frac{1}{4} (1 - \mu^2) \quad (75)$$

For Nwogu's model, WKGS and the variants of the KKCD equations, the coefficients in Eq. (74) are:

$$\begin{aligned}
s_1 &= 2 + \frac{2\mu^2}{1 - \alpha\mu^2} \left[-\alpha - \frac{2}{3} + \alpha \left(\alpha + \frac{1}{3} \right) \mu^2 \right], \\
s_2 &= 3 + \frac{\mu^2}{(1 - \alpha\mu^2)^2} \left[-3\alpha - \frac{10}{3} + 3\alpha(2\alpha + 1)\mu^2 - 3\alpha^2 \left(\alpha + \frac{1}{3} \right) \mu^4 \right], \\
s_3 &= 2 + \frac{2\mu^2}{1 - \alpha\mu^2} \left[-\alpha - \frac{3}{2} + \left(\alpha \left(\alpha + \frac{5}{6} \right) - \frac{1}{3}\zeta - \frac{2\alpha}{3(1 - \alpha\mu^2)} \right) \mu^2 \right], \\
s_4 &= 2 - 4 \left(\alpha + \frac{1}{3} \right) \mu^2 + 2\alpha \left(\alpha + \frac{1}{3} \right) \mu^4, \\
s_5 &= 1 - \left(2 \left(\alpha + \frac{1}{3} \right) + \frac{1}{3} \right) \mu^2 + \alpha \left(\alpha + \frac{1}{3} \right) \mu^4.
\end{aligned} \tag{76}$$

For the MS model, they are:

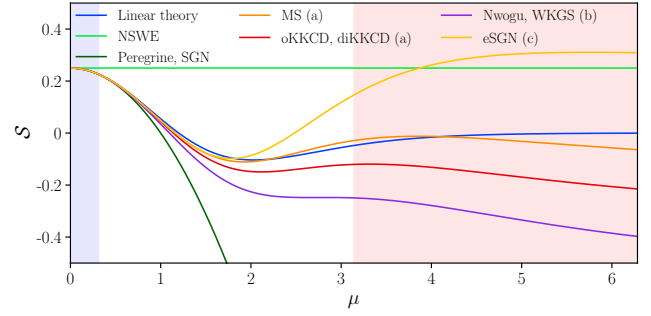
$$\begin{aligned}
s_1 &= 2 \left(1 + 2B\mu^2 + B \left(B + \frac{1}{3} \right) \mu^4 \right), \\
s_2 &= 1 + 6B\mu^2 + 5B \left(B + \frac{1}{3} \right) \mu^4, \\
s_3 &= 1 + \left(4B - \frac{2}{3} \right) \mu^2 + B \left(3B + \frac{2}{3} \right) \mu^4, \\
s_4 &= 2 + 4B\mu^2 + 2B \left(B + \frac{1}{3} \right) \mu^4, \\
s_5 &= 1 + \left(2B - \frac{1}{3} \right) \mu^2 + B \left(B + \frac{1}{3} \right) \mu^4.
\end{aligned} \tag{77}$$

Finally, the coefficients for the eSGN equations are:

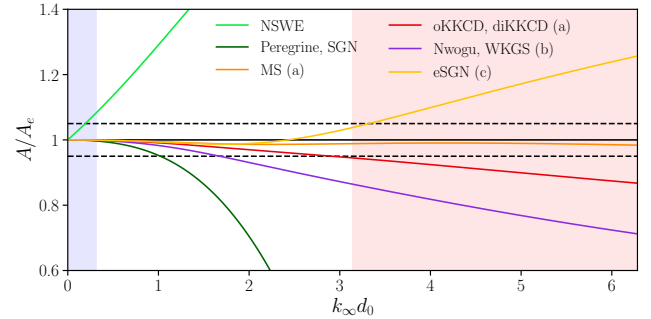
$$\begin{aligned}
s_1 &= 2 + \frac{4}{3}(\gamma - 1)\mu^2 + \frac{2}{9}\gamma(\gamma - 1)\mu^4, \\
s_2 &= -1 + \frac{2}{3}(\gamma - 1)\mu^2 + \frac{1}{3}\gamma(\gamma - 1)\mu^4, \\
s_3 &= \left(\frac{2}{3}\gamma - 1 \right) \mu^2 + \frac{2}{9}\gamma(\gamma - 1)\mu^4, \\
s_4 &= 2 + \frac{4}{3}(\gamma - 1)\mu^2 + \frac{2}{9}\gamma(\gamma - 1)\mu^4, \\
s_5 &= 1 + \left(\frac{2}{3}\gamma - 1 \right) \mu^2 + \frac{1}{9}\gamma(\gamma - 1)\mu^4.
\end{aligned} \tag{78}$$

The linear shoaling gradient for the different models, as well as the one for the NSW (constant and equal to 0.25) and the one obtained from linear theory (Eq. (69)) are plotted in figure 5a. The shoaling gradient for the SGN equations and Peregrine's model considerably underestimates the one from linear theory. The BT models of Nwogu and WKGS have a better shoaling gradient but still underestimate it. For eSGN and MS, the shoaling gradient is close to linear theory until the middle of the intermediate-water range. For deeper waters, it is overestimated for eSGN, while for MS, the agreement is still very satisfactory.

Perhaps, a better way to investigate the linear shoaling properties of the models is to look at the shoaling amplitude at the shoreline as a consequence of cumulative shoaling effect from a deep water location. Following Chen and Liu (1995), for a given wave angular frequency ω and offshore



(a) Linear shoaling gradient for the different models and exact linear wave theory.



(b) Ratio of the linear shoaling amplitude for the models to the one from exact linear wave theory.

Figure 5: Linear shoaling effects for the different models and exact linear wave theory. The blue and red areas represent the shallow- and deep-water ranges, respectively.

water depth d_0 , the ratio of the wave amplitude at the shoreline (where $d = 0$) to the one given by linear theory is:

$$\frac{A}{A_e} \Big|_{d=0} = \exp \left(\int_0^{k_\infty d_0} \frac{S(k_\infty d) - S_e(k_\infty d)}{k_\infty d} d(k_\infty d) \right) \tag{79}$$

with $k_\infty = \omega^2/g$ the deep-water wavenumber from the exact dispersion relation of linear waves. In eq. (79), to compute the local values of the linear shoaling gradients $S(kd)$ and $S_e(kd)$, the local relative depths kd have been expressed as a function of $k_\infty d$ using the linear dispersion relation of the model considered and linear theory. Figure 5b shows the ratio of shoaling wave amplitude for the different models as a function of the incident relative water depth $k_\infty d_0$, with the horizontal dashed lines marking the $\pm 5\%$ error range. This plot confirms that the Peregrine, SGN, Nwogu, WKGS and variants of KKCD models all underestimate linear shoaling. Only the eSGN and MS models keep the error on the shoreline wave amplitude below 5% up to the deep-water range.

However, as already seen with the second-order bound wave amplitude and as will be shown in §5, in a non-linear regime, different behaviours are observed. The MS model considerably underestimates the shoaling of nonlinear waves, as does eSGN to a lesser extent, while Nwogu's and Peregrine's models usually exhibit overshooting.

4. Numerical implementation

The eight model variants were implemented in a single numerical code, solving the various sets of equations in one horizontal dimension (x coordinate) over uneven seabeds. This allows for only investigating the differences between the mathematical models without worrying about the effects of the numerical methods used. A collocated grid with a uniform grid size Δx is used. All spatial derivatives are computed with centred finite differences (FD) with five-point stencils so that formal fourth-order accuracy is achieved for the computation of first- and second-order derivatives, and second-order accuracy for third-order derivatives. Time integration is performed with the standard fourth-order Runge-Kutta explicit scheme, with a fixed time step Δt . For each model, three specific subroutines compute respectively the RHS of Eqs. (3) and (6), the variable K from u , and the velocity u from K . The rest of the code is identical for all models.

Two types of boundary conditions (BC) are implemented: periodic BC and wall (fully reflective) BC. For the periodic BC, the nodes from the other end of the domain are used to compute derivatives near each boundary. For the wall BC, we add a mirror domain, symmetrical to the physical domain and a periodic BC is applied to this extended domain. The symmetry allows for perfect reflection at the boundaries. A sketch of the discretisation and BCs can be found in figure 6. Computations are made on N_x nodes, and in the periodic case (figure 6a) the length of the physical domain is $L = N_x \Delta x$, while in the reflective case (figure 6b), the total periodic domain has a length $2L = 2(N_x - 1)\Delta x$.

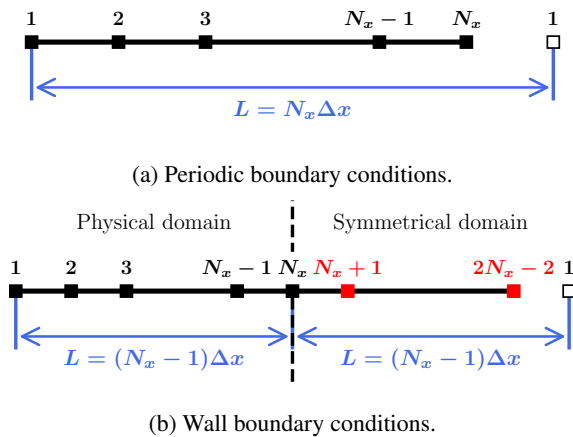


Figure 6: Grid configuration and boundary conditions.

The discretisation of the elliptic equation (7) with five-point stencil FD leads to a linear system with a cyclic pentadiagonal matrix since off-diagonal terms appear due to the periodic boundary conditions. This linear system must be solved at each time step to recover the velocity. We recall that this matrix is time-independent for Nwogu's and

Peregrine's models due to the weakly nonlinear character of these equations. The linear system of equations is solved with the algorithm from Neossi Nguetchue and Abelman (2008). Although this algorithm is very efficient, this step remains the most time-consuming in the resolution process of the governing equations.

For the first test case of the next section, wave generation and absorption are needed. The generation is performed with the widely used source function method from Wei et al. (1999). It consists of adding a distributed source term on the RHS of the mass conservation equation of the form:

$$f(t) \exp\left(-\beta_g (x - x_c)^2\right) \quad (80)$$

x_c is the desired centre of the generation zone, and β_g controls the length of this zone. Following Wei et al. (1999), $\beta_g = 80/(\Delta\lambda_p)^2$ with λ_p the local peak wavelength and Δ a parameter that can be adjusted to improve the quality of the generated wave train. With this expression, the total length of the source function is approximately $\Delta\lambda_p/2$. Although $\Delta \in [0.3, 0.5]$ is recommended in Wei et al. (1999), choosing a value in the interval $[4, 5]$ was found to give a more satisfactory shape for the generated signal. Following Kim et al. (2007), the amplitude of the source function is based on the group velocity of the model $C_g = \partial\omega/\partial k$, and is written for monochromatic waves:

$$f(t) = \frac{2C_g a}{I} \sin(\omega t) \quad (81)$$

with a the desired wave amplitude. The term I is here to normalise the Gaussian shape function (80) and is defined as:

$$I = \sqrt{\frac{\pi}{\beta_g}} \exp\left(-\frac{k^2}{4\beta_g}\right) \quad (82)$$

with k computed from the linear dispersion relation of the model.

Wave absorption is performed with relaxation zones of length L , typically of the order of one wavelength, in which at each location x , the free surface elevation η and the auxiliary variable K are attenuated by multiplying them by a coefficient $C_r(x)$, expressed as (Kazolea et al., 2023):

$$C_r(x) = \sqrt{1 - \left(\frac{x - x_s}{L}\right)^2} \quad (83)$$

with x_s the position of the interface between the relaxation zone and the rest of the domain.

Finally, except for some situations discussed in subsection 5.1 hereafter, no smoothing nor filtering was applied during all the simulations reported in the next section.

5. Comparison of the models

The numerical code has been used to compare the eight model variants on three wave propagation cases. The parameter choices for the wave models are those given in the

references in which the models were derived, namely choice (a) for MS, oKKCD and diKKCD, choice (b) for Nwogu and WKGS, and choice (c) for eSGN (see §3.1 where the parameter values are given). Although other optimisation strategies could be chosen, as pointed out by Choi et al. (2015), slight variations usually do not significantly influence the results. They simulated the experiments of shoaling and breaking of random waves from Mase and Kirby (1992) with the equations of Nwogu (1993) and two different optimisation strategies, obtaining results closer to each other than to the experimental data regarding various wave statistics. The approximate nature of the models and errors in the bathymetry and/or the input wave and boundary conditions probably contribute more to deviations from the observations than a suboptimal parameterisation of the models, at least when weakly to mildly dispersive waves are considered.

5.1. Case 1: Regular waves over a submerged bar

The first case considered is case A of the wave flume experiments of Dingemans (1994). It consists of the propagation of non-breaking regular waves of period $T = 2.02$ s and amplitude $a_0 = 1$ cm over a submerged trapezoidal bar. The setup is shown in figure 7. This is a popular test case because nonlinear energy transfers combined with important dispersive effects are observed. In the upwave flat region of still water depth 0.4 m, the waves have a wavelength $\lambda \approx 3.8$ m, thus incident waves are characterised by $\mu \approx 0.67$ and $\varepsilon = 0.025$. Relaxation zones of length λ are used on both ends of the computational domain to absorb the waves, and we choose $\Delta = 5$ for the source function width for all models except WKGS, for which we choose $\Delta = 4.5$. With this value, the generated waves are the most satisfactory, with a constant height when propagating and as few higher and lower harmonics generated as possible. We observed that using a larger value of Δ for WKGS was impossible without triggering trough instabilities in the generation zone, leading to the solution blowing up. Using $\Delta = 4.5$ in WKGS, the generated wave train is still satisfactory.

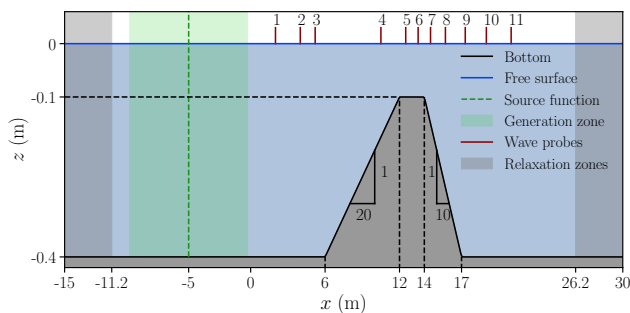


Figure 7: Case 1 - Bathymetry and numerical setup for the simulation of case A of the experiments of Dingemans (1994), with the location of the wave probes.

The waves propagate and shoal over the upslope of the bar, leading to energy transfers to bound higher harmonics since they become more and more nonlinear as

the water depth is reduced. These harmonics are then released over the plateau of the bar and mainly its downslope due to the sudden changes in the bottom slope as unveiled by Eldrup and Lykke Andersen (2020). A fine grid size of $\Delta x = 1$ cm $\approx \lambda/380$ is used to resolve correctly these super-harmonics. Similarly, a small time step $\Delta t = 2.5$ ms $\approx T/808$ is used. The maximum Courant number with all the BT models is approximately $Co = 0.55$. It is here defined as:

$$Co = \frac{\Delta t}{\Delta x} \max_i \left(|u_i| + \sqrt{gh_i} \right) \quad (84)$$

with i running over the mesh nodes indices.

Before comparing all models' results, we discuss the particular case of the Peregrine and SGN models. Indeed, we observed in this test case that both these models struggle to model the free higher harmonics due to their limited dispersive properties. It manifests itself through short-wavelength oscillations generated on the downslope of the bar when these harmonics are released (as illustrated for the SGN model in Figure 9(a), discussed hereafter). These oscillations probably have a low phase speed and do not seem to propagate. Therefore, they accumulate in the course of the simulation, and the solution eventually blows up for long simulation times. This is not due to a lack of numerical dissipation, as increasing Δx or Δt did not prevent them from appearing. Although using another numerical method could mitigate these effects, we note that similar observations on the shortcomings of the SGN equations were made in Mihami (2023) when used to simulate these experiments. To alleviate the growth of these perturbations and obtain a steady signal in the domain, a fourth-order Savitzky-Golay (SG) filter, using a sliding 9-point stencil, is applied four times per wave period (i.e. every $202\Delta t$) to η and K between $x \in [14$ m, 18 m]. Figure 8 shows the time series of free surface elevation at $x = 16.2$ m, where the strongest oscillations are generated, for the SGN equations with and without applying the SG filter (a similar behaviour was observed with Peregrine model, thus not duplicated here). It is apparent that without filtering, the amplitude of the oscillations grows in time, while with filtering, a steady signal is reached after roughly $t = 30T$.

Figure 9 shows a snapshot of the free surface over the downslope at $t = 40T$ obtained with the SGN equations without and with filtering. The SG filter has effectively damped the short oscillations and prevented the accumulation of perturbations for $x \in [16$ m, 17 m]. Note that the oscillations happen between probes 8 and 9 (and do not propagate), so the filtering barely affects the time series at the wave probes. As already mentioned, Peregrine's model showed similar behaviour, and in the following, the results displayed with both models are obtained with the application of the SG filter four times per T .

We now show some free surface elevation time profiles at some wave probes in figure 10. The results with the weakly nonlinear models of Nwogu, Peregrine and MS are plotted with solid lines, WKGS and the variants of KKCD with dash-dotted lines, and the variants of the SGN equations with

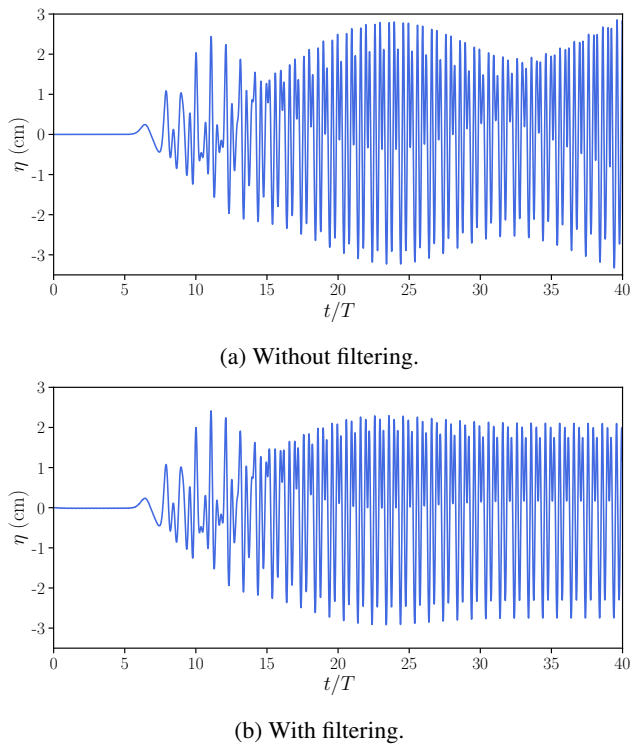


Figure 8: Case 1 - Time series of free surface elevation for the SGN equations at $x = 16.2\text{m}$ without and with applying the SG filter.

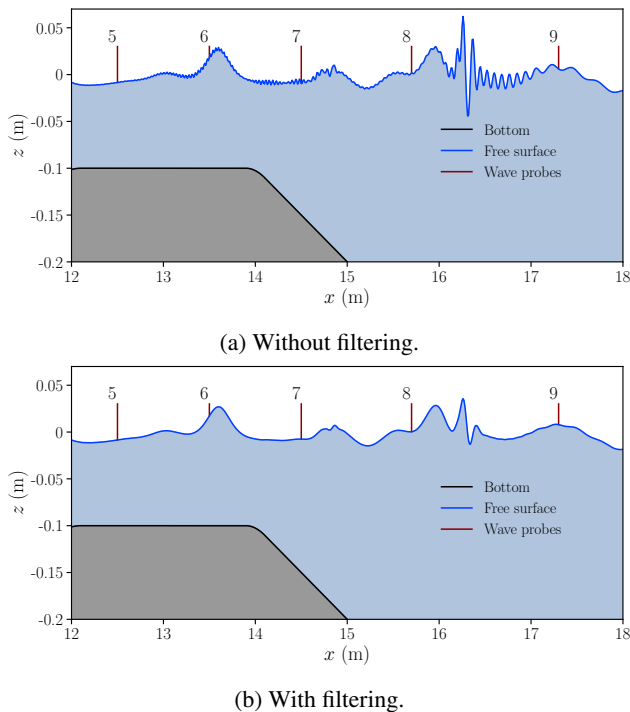


Figure 9: Case 1 - Snapshots of free surface elevation for the SGN equations at $t = 40T$ without and with applying the SG filter.

dashed lines. Probe 6 shows that after the shoaling phase, the wave train is qualitatively well reproduced by all the

models, except for the primary peaks, for which we see some overshooting with most models. The models overestimating the most the free surface peak are the Nwogu and Peregrine models, then WKGS and oKKCD, and finally, diKKCD and eSGN overestimate it only slightly. With SGN and MS models, the height of the peak is rather well predicted. As shown by Eldrup and Lykke Andersen (2020), some of the bound harmonics generated are released over the top of the bar, but probably in a small proportion due to the short length (2 m) of the area, and in these shallow water conditions, they are not too dispersive and are modelled correctly by all models. Bound energy is further released over the downslope of the bar, and we can see at probe 8 essentially two behaviours: that of the models without any enhancement of their dispersive properties (Peregrine and SGN) and that of the dispersion-enhanced models. The shape of the wave train predicted by the Peregrine and SGN models is very similar, despite the full nonlinearity of the SGN equations, and is considerably different than in the experiments because a significant proportion of the incident energy has shifted to higher harmonics with high relative water depths μ , too important for the models to handle due to their limited dispersive properties. For the other models, the wave shape is well predicted, with a slight phase advance and, again, some overestimation of the height of the peaks, but the differences between the models are not so significant. More discrepancies can be observed at the two last probes (10 and 11). The free harmonics are highly dispersive waves that are not well resolved by any weakly dispersive models considered here. The SGN and Peregrine models can again not match the experimental free surface time series, and all the dispersion-enhanced models show a phase shift compared to the experimental data. The eSGN model seems to be the most in phase with the experiments. The oKKCD and diKKCD models give almost identical results, but other than that, all models predict different wave shapes and crests and troughs elevations. By just looking at these free surface elevation time series, it is difficult to determine whether some models perform better than others.

To better visualise how the different models reproduce the nonlinear energy transfers, we examined the spatial evolution of the harmonics amplitudes of free surface elevation. In figure 11, we show these variations for the first four harmonics for all the models, with the experimental data represented as black dots. Before the bar, most of the energy is carried by the primary component, and all models predict similar amplitudes due to the only weak dispersive and nonlinear effects. The amplitude of the harmonics is modulated due to the reflection on the bar of some of the incident energy. During the shoaling phase, the amplitude of the four harmonics increases due to the decreasing water depth and increasing nonlinear energy transfers. Over the top of the bar, for $x \in [12\text{ m}, 14\text{ m}]$, a considerable amount of the energy of the first harmonic is transferred to higher harmonics. After the downslope, all the amplitudes are relatively constant and modulated due to the presence of free waves released over the back of the bar, in addition to the bound components. The

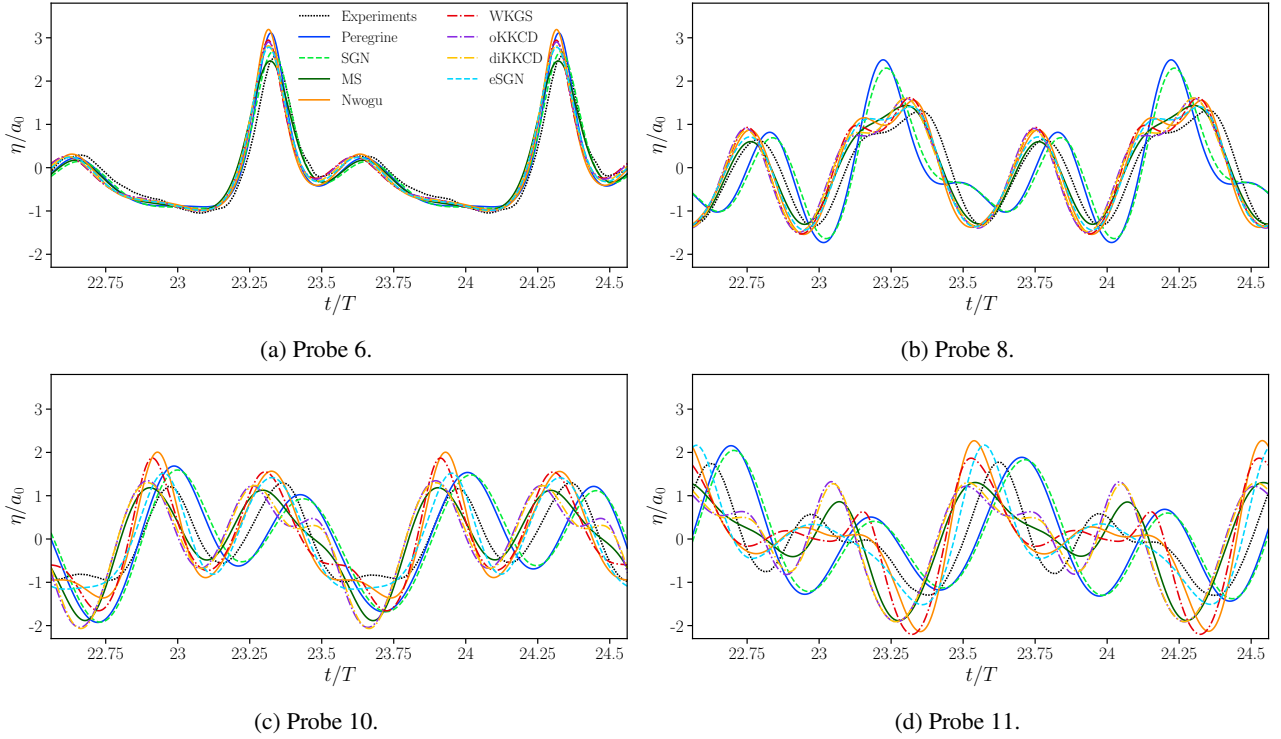


Figure 10: Case 1 - Free surface profiles at probes 6, 8, 10 and 11.

amplitude of the first harmonic is very similar for all models except for the SGN and Peregrine models, which again give almost identical results. Differences appear at the downslope for harmonic $2f$ and at the top of the bar for $3f$ and $4f$. Due to the oscillations mentioned earlier, some perturbations are observed on the first and second harmonics for the SGN and Peregrine models towards the end of the downslope. The amplitude of harmonic $2f$ is overestimated by all models after the bar, more importantly by the Peregrine, SGN and Nwogu models. The amplitude of harmonic $3f$ is slightly overestimated by the WKGS, KKCD and Nwogu's model, and underestimated by the MS model. eSGN predicts well the amplitude at all wave probes. For the SGN equations and Peregrine's model, we notice a significant and sudden increase in the amplitude of the harmonic at the end of the downslope where it is released. According to the analysis of the linear properties of the models in §3.1, the phase speed of the highly dispersive free harmonic should be substantially underestimated, and it does not propagate, probably explaining that its amplitude plummets immediately afterwards and is considerably underestimated after the bar. Similarly, for the harmonic $4f$, the amplitude is underestimated by MS at the top of the bar and overestimated by the other models, mainly by Nwogu's. After the bar, the amplitude varies significantly, and eSGN is again the most accurate model. For the SGN and Peregrine's models, as observed for the harmonic $3f$, the amplitude of harmonic $4f$ peaks at the end of the downslope but also a smaller one at its beginning, and the amplitude is underestimated after the bar.

This case has allowed us to showcase how the different models behave when strong dispersive effects come into play. The models without any enhancement of their dispersive properties can not deal with such a situation due to the important underestimation of the phase speed for deep water waves. The SGN equations and Peregrine's model give almost identical results, although the former is fully nonlinear and considerably more complicated than the latter. The improved models, although incapable of reproducing precisely the behaviour of strongly dispersive free harmonics after the bar, still provide acceptable results regarding the lowest order harmonics and the overall shape of the wave train.

5.2. Case 2: Unsteady shoaling of a wave train

The second case, put forward by Kennedy et al. (2001), consists of the unsteady shoaling of a wave train over a variable seabed. The bathymetry is shown in figure 12 together with the initial free surface elevation. The bathymetry is specified through the still water depth as:

$$\frac{d}{d_1} = \begin{cases} \frac{d_{\min}}{d_1} + \frac{1 - d_{\min}/d_1}{\cosh(\tan(\pi x/(2L)))} & x_L \leq x \leq L \\ \frac{d_{\min}}{d_1} & L < x \leq x_R \end{cases} \quad (85)$$

with d_1 the still water depth in the deepest (i.e. left) part of the domain, and d_{\min} the still water depth in the shallowest (i.e. right) part. Here, $d_{\min}/d_1 = 0.2$, $x_L = 0$, $x_R = 74d_1$ and $L = 50d_1$. Lateral boundary conditions are vertical

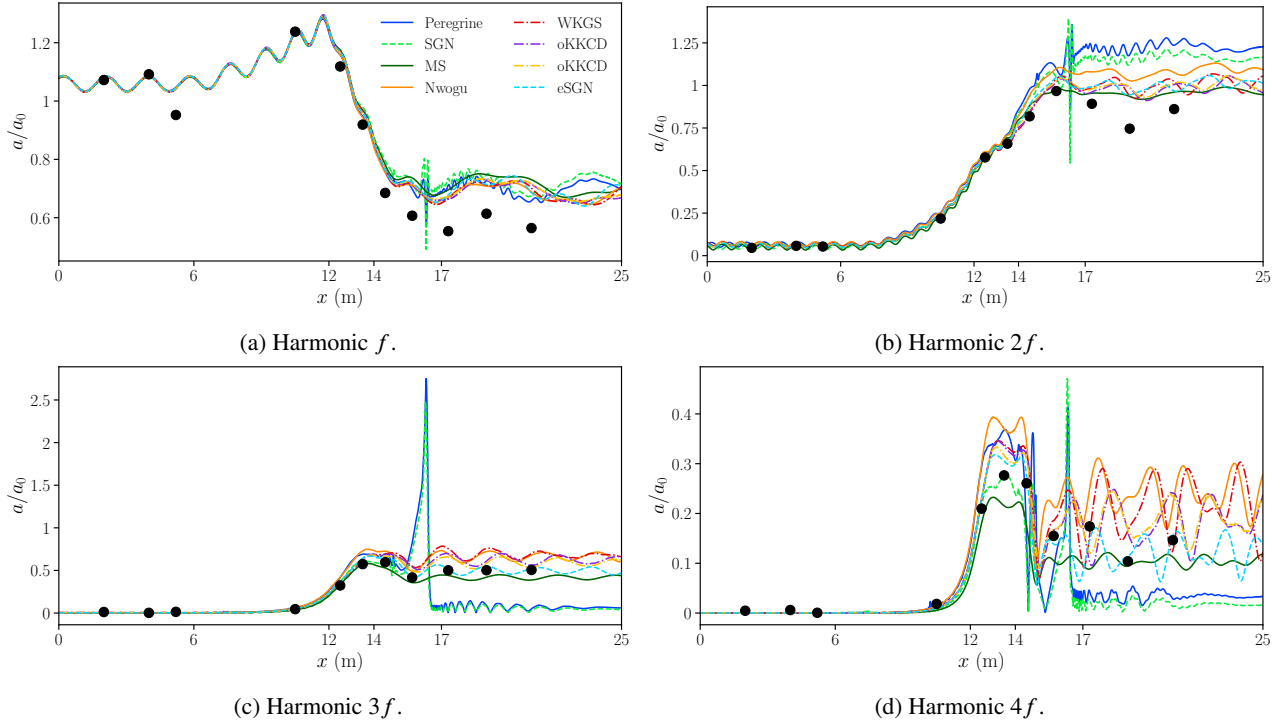


Figure 11: Case 1 - Spatial variations of the amplitude of the first four harmonics for all the models. The black dots are the amplitudes computed from the experimental data at the eleven probes.

(fully reflective) walls. The initialisation consists of a tapered pseudo-regular wave train:

$$\frac{\eta}{d_1} = \frac{a_1}{d_1} \left[\frac{\cos(2\pi N x/L)}{\cosh(\tan(\pi x/(2L)))} \right] \quad (86)$$

with zero velocity inside the whole fluid domain. We consider the case 1 in Kennedy et al. (2001), with $N = 10$ and initial wave nonlinearity $a_1/d_1 = 0.125$ in eq. (86).

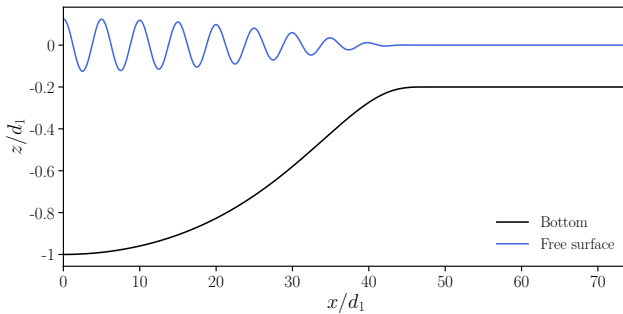


Figure 12: Case 2 - Initial free surface elevation and bathymetry of case 1 in Kennedy et al. (2001), with the fluid domain entirely at rest at initial time.

Close to the left wall, the wave train evolves similarly to a standing wave while it becomes rapidly progressive in its rightmost front and shoals over the variable seabed. The wavelength being $\lambda = L/N = 5d_1$, the relative water depth in the deepest region is $\mu \approx 1.3$. Linear dispersive properties of all models, except the SGN equations and the

BT model of Peregrine, are expected to be accurate at such depths. The simulation was stopped at the dimensionless time $t\sqrt{g/d_1} = 45$ following Kennedy et al. (2001), as the leading waves in the shallowest region were deemed near breaking.

In this test, we focus on the envelopes of minimum and maximum free surface elevation over the time range $t\sqrt{g/d_1} \in [0, 45]$. Table 3 gives the maximum absolute error on the envelope of crest elevation for the eight models and four decreasing dimensionless grid size $\Delta x/d_1$, compared to the solution obtained with $\Delta x/d_1 = 0.005$ (specific to each model considered).

Based on the results of this convergence study, a grid size of $\Delta x/d_1 = 0.02$ is used for all models but WKGS, giving at most 4×10^{-4} difference on the dimensionless crest envelope compared with the solution obtained with $\Delta x/d_1 = 0.005$. For the WKGS model, mesh convergence is not reached as described below, and $\Delta x/d_1 = 0.005$ is used to display the results. The chosen time step is $\Delta t\sqrt{g/d_1} = 3.1 \times 10^{-3}$ for WKGS, and 4×10^{-3} for the other models, giving a maximum Courant number of approximately 0.67.

No experimental data is available for this test case, and the reference solution is obtained here with the fully dispersive, fully nonlinear potential flow (FNPF) model whispers3D, which solves the Zakharov formulation of the potential flow equations with a spectral approach in the vertical (Zhang et al., 2019; Zhang and Benoit, 2021; Zhang et al., 2022). The solution was obtained with this solver after a convergence study and was almost identical to the one obtained in Kennedy et al. (2001) with another FNPF solver.

Model	$\Delta x/d_1 = 0.1$	$\Delta x/d_1 = 0.04$	$\Delta x/d_1 = 0.02$	$\Delta x/d_1 = 0.01$
Peregrine	6×10^{-3}	3×10^{-4}	2×10^{-5}	10^{-6}
SGN	2×10^{-3}	8×10^{-5}	5×10^{-6}	3×10^{-7}
MS	2×10^{-3}	2×10^{-4}	4×10^{-5}	7×10^{-6}
Nwogu	9×10^{-3}	4×10^{-4}	3×10^{-5}	2×10^{-6}
WKGS	4×10^{-2}	2×10^{-2}	10^{-2}	9×10^{-3}
oKKCD	2×10^{-2}	3×10^{-3}	4×10^{-4}	4×10^{-6}
diKKCD	7×10^{-3}	4×10^{-4}	3×10^{-5}	2×10^{-6}
eSGN	6×10^{-3}	3×10^{-4}	2×10^{-5}	10^{-6}

Table 3

Case 2 - Maximum error on the envelope of crest elevations η_{\max}/d_1 compared to the solution with $\Delta x/d_1 = 0.005$ for different grid sizes and each model.

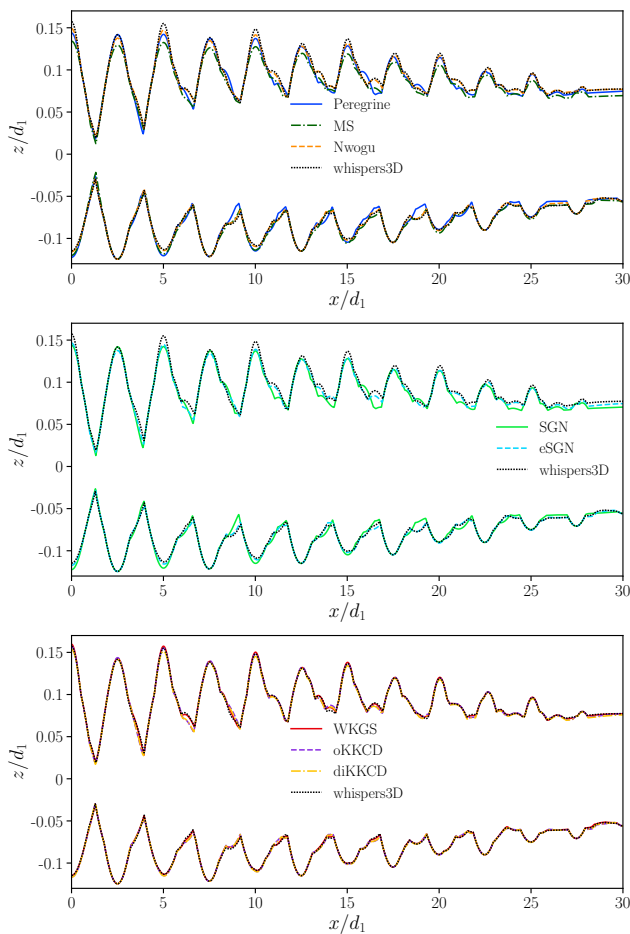


Figure 13: Case 2 - Crests and troughs envelopes in the left part of the domain, computed in the time range $t\sqrt{g/d_1} \in [0, 45]$.

Figures 13 and 14 show the envelopes of wave crests and troughs during the whole simulation for all eight models plus the whispers3D reference solution. Figure 13 shows the results for $x/d_1 \in [0, 30]$ (left part of the domain), and figure 14 for $x/d_1 \in [30, 60]$ (right part). The envelopes are split over three sub-figures, each with the reference solution, for better visualisation: the top panel with the

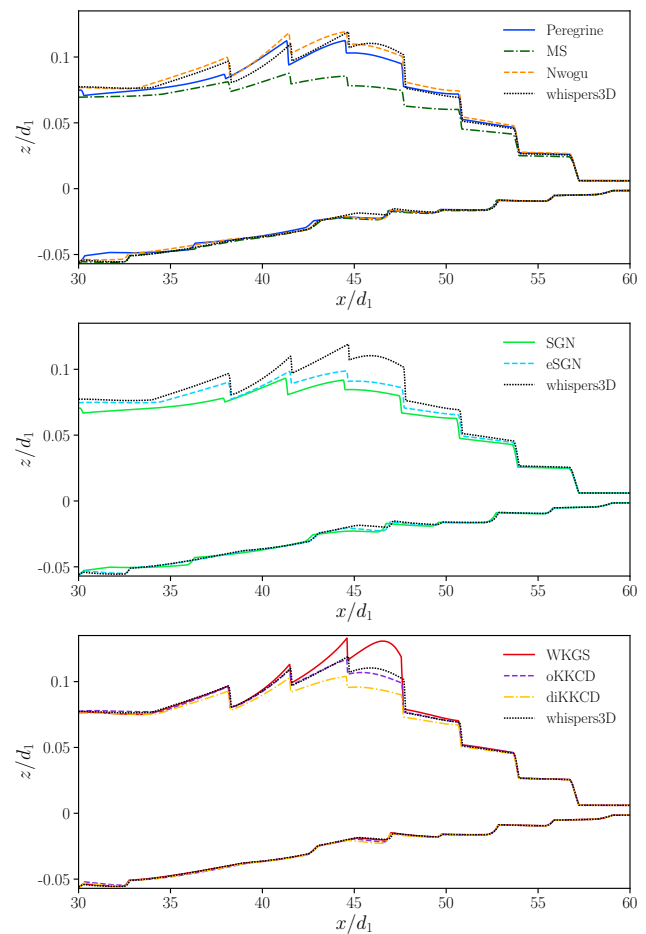


Figure 14: Case 2 - Crests and troughs envelopes in the right part of the domain, computed in the time range $t\sqrt{g/d_1} \in [0, 45]$.

weakly nonlinear models, the middle one with the two variants of the SGN equations, and the last one with the variants of WKGS and KKCD models. As shown in figure 13, all wave envelopes are pretty close to each other, except the MS model, which underestimates crest elevations. This shows that the dispersive effects in the deeper part of the

domain and the beginning of the shoaling phase are generally well captured by all models. More significant discrepancies appear between the models towards the end of the slope and the shallowest region in the right part of the domain (figure 14). The envelopes exhibit near vertical fronts because they are the last waves reaching the shallowest area that shoal the most and have the highest crest elevation and steep fronts. The maximum crest elevation is then given by the elevation of the last wave crest reaching each location. In figure 14, the wave trough elevations are quite well predicted with minor differences among the various models (in contrast to wave crest envelopes). With Nwogu's model, the maximum crest elevation is overestimated everywhere except for $x/d_1 \in [45, 48]$ approximately. WKGS model also overestimates crest elevations: the higher the crest elevation in the reference solution, the more it is overestimated, as can be seen for $x/d_1 \in [42, 48]$ approximately. With Peregrine's model, as with Nwogu's, crest elevations are overestimated or underestimated depending on the location. The oKKCD equations give the best results, in line with the findings of Kennedy et al. (2001). All other models consistently underestimate the maximum crest elevation, and from the closest to the furthest from the reference solution, we have diKKCD, eSGN, SGN and MS.

Although they gave the best results for the previous test case, the eSGN equations underestimate the wave crest envelope so significantly that they provide worse results than the weakly nonlinear models of Nwogu and Peregrine, even though the latter has limited dispersive properties. It should be noted that at the end of the calculation, the maximum wave height corresponding to the crest located at $x/d_1 \approx 44$ and computed with whispers3D is $H/d_1 \approx 0.14$, giving a local nonlinearity ratio $\varepsilon = H/(2d) \approx 0.33$ which is very high. The wave conditions are then far beyond the assumption of moderate amplitude theoretically required for weakly nonlinear models, and the seemingly better results obtained with Nwogu's and Peregrine's models compared to the SGN and eSGN models are surprising. As mentioned, the highest waves approach the breaking onset at the end of the simulation (with the reference FNPF model), and since the wave height is not very well estimated with most models, then neither the breaking location nor the breaking strength, related to the wave height at the breaking onset, will be predicted accurately with these approximate models. As noted by Kennedy et al. (2001) for the variants of WKGS and KKCD models, all BT models predict locations for crest envelope fronts further upstream than whispers3D, meaning they all underestimate the phase speed of the most nonlinear waves, which is different from what was observed in the linear framework in §3.1.

It was noted in Figure 14 that the WKGS model produces excessive shoaling of the highest waves. As pointed out by Kennedy et al. (2001), when decreasing the grid size to try to reach mesh convergence with this model, the maximum wave crest elevation for $x/d_1 \in [45, 48]$ approximately consistently increases and convergence is never reached. Figure 15 shows the crest envelope over the range $x/d_1 \in$

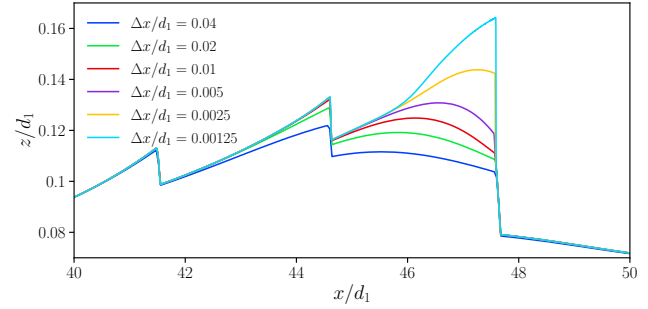


Figure 15: Case 2 - Crest envelopes with WKGS model for 6 grid sizes shown over the reduced range $x/d_1 \in [40, 50]$.

$[40, 50]$ for 6 decreasing grid sizes (including values lower than the ones used in Table 3). Mesh convergence is approximately reached for $\Delta x/d_1 = 0.01$ outside this range. However, the elevation of the last wave crest reaching this range continuously grows for decreasing grid size.

Some insight on what causes this can be gained from figure 16 showing the crest elevation of the troublesome wave at three instants towards the end of the simulation and for three grid sizes. For each grid size, the Courant number is $C \approx 0.35$. At $t\sqrt{g/d_1} = 41$, the wave is very peaked, such that breaking is incipient, but mesh convergence appears to be reached with $\Delta x/d_1 = 0.005$. A spurious peak appears later for the two finest grid sizes and grows in amplitude until the simulation is stopped. This uncontrolled growth is probably due to dispersive terms reaching unphysical values and the crest being too sharp. The results presented in figures 13 and 14 are the ones with the grid size that ensures mesh convergence for the rest of the simulation, $\Delta x/d_1 = 0.005$. As a take-way message, as already pointed out by Kennedy et al. (2001), it appears preferable to use one of the versions of the KKCD model proposed by these authors rather than the original WKGS from Wei et al. (1995), which overestimates shoaling effects in this case and predicts premature breaking of the highest wave.

5.3. Case 3: Propagation, shoaling and run-up on a vertical wall of a wave train

The third test case was put forward by Benoit et al. (2018) to assess the suitability of a large range of numerical models for the simulation of tsunami-type wave trains. Dispersive and nonlinear effects come into play, making it appropriate for our purpose. The geometry is represented in figure 17. The domain is 30 km long, with first a flat region of 25 km, then a foreshore slope of 1 : 125 over a distance of 4 km, a final 1 km flat reef and vertical walls on both sides. The case consists of the generation and propagation over a long distance of a dispersive shock wave (DSW)—or undular bore—from an initial disturbance, showing weakly to mildly dispersive effects. The analytical expression for the initial

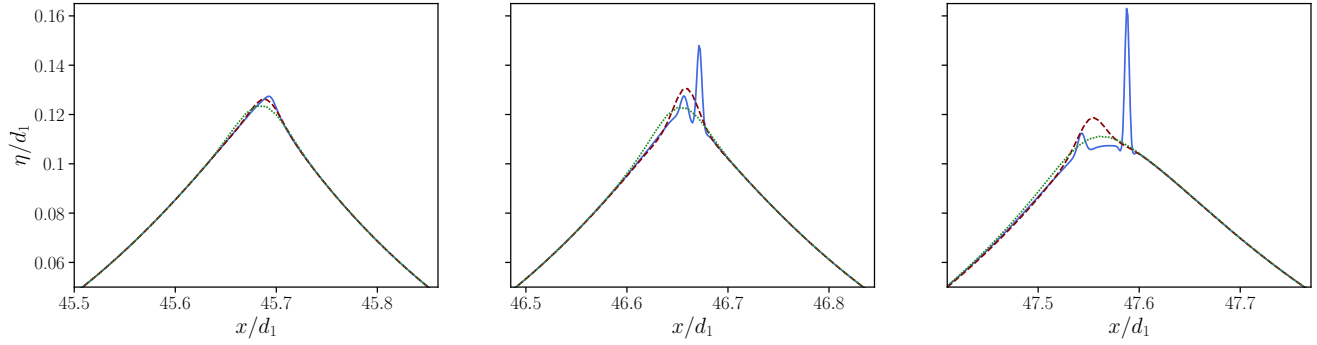


Figure 16: Case 2 - Free surface profiles at $t\sqrt{g/d_1} = 41, 43.1$ and 45 from left to right for WKGS model with 3 grid sizes: solid blue line: $\Delta x/d_1 = 0.00125$, dashed red line: $\Delta x/d_1 = 0.005$, and dotted green line: $\Delta x/d_1 = 0.01$.

free surface profile is:

$$\eta(x) = \begin{cases} 5 \text{ m} & x \leq 1.9 \text{ km} \\ 0 \text{ m} & x \geq 2.1 \text{ km} \\ 2.5 \left(1 - \tanh\left(\Delta\left(\frac{x}{x_0} - 1\right)\right)\right) & \text{elsewhere} \end{cases} \quad (87)$$

with $\Delta = 229.756$ and $x_0 = 2 \text{ km}$. The initial velocity is null throughout the domain. The generated wave train propagates towards the right wall, shoals over the variable seabed and is thus affected by nonlinear effects, and finally runs up the right wall and is reflected.

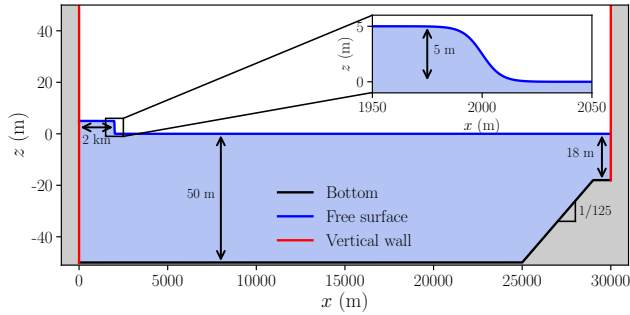


Figure 17: Case 3 - Geometry, initial condition and boundary conditions.

The simulation time is 1 hour of physical time so that the leading waves have time to reflect on the right wall, travel back towards the left wall, and run up. The solution obtained with whispers3D again serves as a reference. In Benoit et al. (2018), this solution was found to be almost identical to the one obtained with two other codes solving the FNPF equations with different numerical methods, so there is strong confidence that whispers3D accurately predicts the FNPF solution. The solution computed with a code based on the NSWE is also shown to highlight the importance of dispersion in this case.

One of the most discriminating features of this case is the value of the maximum run-up height on the right wall (MRHRW), as shown in figure 24 and table 5 discussed below, and this variable is used as a proxy when performing convergence studies and selection of discretisation parameters. Table 4 shows the relative error on MRHRW for

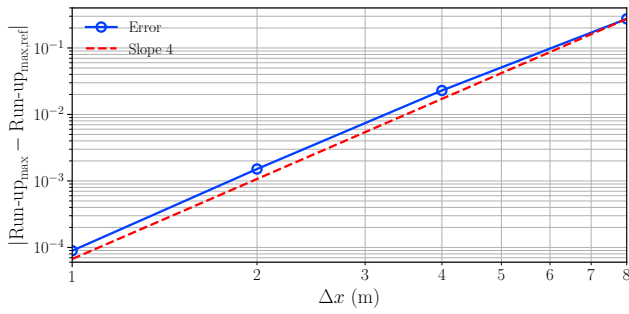
Model	$\Delta x = 8 \text{ m}$	$\Delta x = 4 \text{ m}$	$\Delta x = 2 \text{ m}$	$\Delta x = 1 \text{ m}$
Peregrine	2.1	0.18	0.012	0.00069
SGN	1.13	0.089	0.0059	0.00035
MS	0.37	0.045	0.0078	0.0014
Nwogu	2.6	0.23	0.016	0.00092
WKGS	8.7	1.6	0.11	0.0033
oKKCD	6.3	0.83	0.043	0.0015
diKKCD	3.5	0.35	0.021	0.0021
eSGN	1.5	0.12	0.0079	0.00046

Table 4

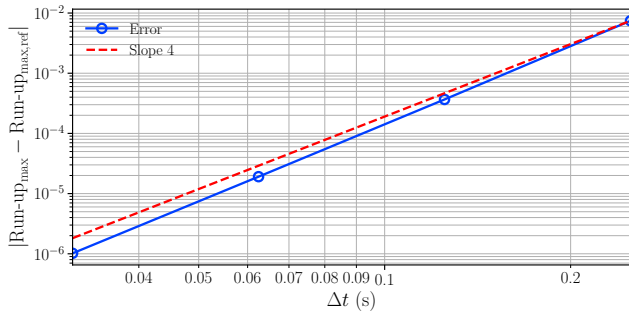
Case 3 - Relative error (in %) on the MRHRW, compared to the solution with $\Delta x = 0.5 \text{ m}$ for different grid sizes and each model.

the eight models and different grid sizes, compared to the solution obtained with each model with $\Delta x = 0.5 \text{ m}$. For a given grid size, WKGS consistently shows the highest errors, up to two orders of magnitude higher than the lowest errors. Although this probably depends on the way the dispersive terms are written and the numerical methods used, this indicates that, depending on the model, mesh-independent results can be achieved with quite different grid sizes. Based on these errors, the chosen grid size for the computations with all the BT models is $\Delta x = 2 \text{ m}$. For all models, the error on the predicted maximum run-up on the right wall is lower than 3 cm or 0.11%. The chosen time step is $\Delta t = 0.0625 \text{ s}$ to accurately capture the sharp run-up peak on the right vertical wall. The maximum Courant number for the simulations with the BT models with the chosen time step is approximately 0.78. Figure 18 shows the convergence of the MRHRW for decreasing grid sizes (panel (a)) and time steps (panel (b)) and for the eSGN model. One can check that the present numerical scheme achieves fourth-order convergence in time and space. Similar convergence orders were obtained with all the BT models and are not shown here for conciseness.

With the grid and time steps that were selected above ($\Delta x = 2 \text{ m}$, $\Delta t = 0.0625 \text{ s}$), we first look at snapshots of the



(a) Grid convergence.



(b) Time step convergence.

Figure 18: Case 3 - Mesh and time step convergence of the maximum run-up height on the right wall (MRHRW) for the eSGN model. The reference solutions are computed with $\Delta x = 0.5$ m and $\Delta t = 0.015625$ s for the mesh convergence, and $\Delta x = 2$ m and $\Delta t = 0.015625$ s for the time step convergence.

free surface at $t = 30$ s, 5 min, 15 min and 21 min. Figure 19 shows the free surface profiles of the reference solution over the whole domain at those four instants. From the initial condition, a DSW propagating towards the right is formed, as can be seen at $t = 30$ s. The wave train then propagates towards the right, shoals, and reaches the wall a little after $t = 21$ min.

We now compare the profiles for the various BT models in figures (figs. 20 to 23). Again, the free surface profiles are split over three figures, each with the reference solution, for better visualisation: one with the weakly nonlinear models and the NSW, one with the two variants of the SGN equations, and one with the variants of WKGS and KKCD. At $t = 30$ s, the leading wave on the right is well reproduced by all BT models, but the following waves deviate from the reference solution, probably because the dispersive properties of the models are not sufficient to model the short waves generated. Since the NSW are non-dispersive, no undulations appear, and the solution is a right-moving shock (light blue solid line).

At $t = 5$ min (figure 21), the leading waves have propagated over a few kilometres and are very close to the reference solution for all BT models. This is because the first wave has a wavelength of approximately 600 m, so $\mu \approx 0.52$ and all models have sufficient dispersive properties for such relative depths. The following waves are shorter and therefore more dispersive, as $\mu \approx 1.3$ for the shorter

waves on figure 21. These trailing waves propagate at a lower phase speed than the reference solution, particularly for the Peregrine and SGN models, which have the most limited dispersive properties. The same is true for the MS model despite it having enhanced dispersion.

At $t = 15$ min (figure 22), the leading waves have almost reached the region with sloping seabed. Wave amplitudes are slightly overestimated with Nwogu's and Peregrine's models, with a slight phase advance. At least for the relative water depth considered, the amplitude overestimation with Peregrine's model compensates for the phase lag previously noticed due to its dispersion limitations. With the MS and SGN models, there is again a phase delay, especially for the trailing shorter waves. In addition, the MS model underestimates wave heights a little. Overall, all BT models propagated the leading part of the wave train with acceptable to good accuracy, as shown in figure 22(b).

Figure 23 shows the leading waves at $t = 21$ min in the final flat region after the shoaling phase, where the nonlinear effects have been handled quite differently by the models. The elevation of the crest of the leading wave is about 9.5 m with whispers3D (in a still water depth of 18 m); thus, nonlinearity is very high. The overestimation of the wave amplitude and the phase advance previously observed with Nwogu's and Peregrine's models are more pronounced now for all the waves, as the elevation of the first crest is around 1 m too high with these models. WKGS overestimates this elevation by 0.4 m approximately, and the oKKCD solution is almost superimposed with the reference solution. diKKCD, eSGN, SGN and MS underestimate the elevation by 0.2 m to 1.4 m in that order, with a slight phase lag. The NSW severely underestimate the wave height by around 6.4 m. Some phase delay is again present with MS and SGN equations for the shorter waves.

We then look at the MRHRW, with figure 24 showing the time series of the run-up on the right wall. Figure 24a shows the run-up of the leading waves for all models, and the run-up peak for the different models is then shown over the three figures 24b, 24c and 24d. The same trends in elevation and phase delay noticed in figure 23 for the models can be seen. The signal is qualitatively well reproduced by all the dispersive models, while the NSW predict a flat run-up peak with a slight phase delay and an elevation underestimated by almost 75 %. In figure 24a, except for the first wave with the largest amplitude, all fully nonlinear models are very close to the reference solution, even if a slight phase lag remains for the SGN equations (which have more limited dispersive properties compared to the others). The models from Nwogu and Peregrine systematically predict higher and earlier peaks. MS model deviates less from whispers3D, but some discrepancies can be observed. Full nonlinearity then gives noticeable improvements here. More differences appear when looking at the run-up peak with the first wave. Table 5 shows the MRHRW for all models, as well as the relative error with the reference value of 24.41 m predicted by whispers3D. The run-up signal on the right wall was recorded at each time step, and the maximum value was

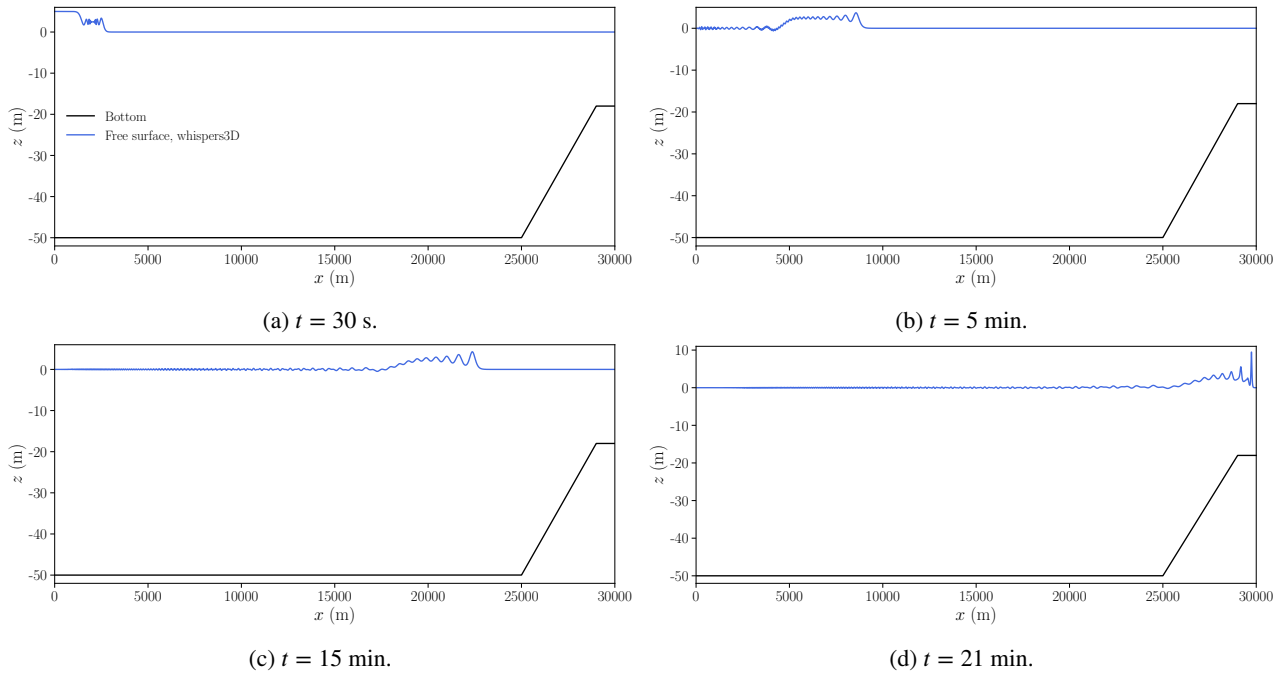


Figure 19: Case 3 - Free surface profiles of the reference solution at $t = 30$ s, 5 min, 15 min and 21 min.

found by cubic interpolation on a finer time discretisation. The weakly nonlinear models of Peregrine and Nwogu predict the run-up peak 1.5 to 2 s earlier than whispers3D. Although they predicted a too-high amplitude for the leading wave before run-up, they underestimated the MRHRW by 5 to 7 %. The peak with the MS model is almost in phase but considerably underestimated (≈ 29 %). The same can be observed for the SGN and eSGN equations, with a relative error of -16 and -17 % on the MRHRW, respectively. Finally, WKGS, oKKCD and diKKCD are the closest to the reference signal. WKGS overestimates the MRHRW by ≈ 5 %, diKKCD underestimates it by ≈ 7 %, and oKKCD predicts a peak value within 0.1 % of the reference one. The wave train then de-shoals, propagates towards the left wall and runs up. After de-shoaling the leading waves are similar for the different models, as noted by Kazolea and Ricchiuto (2024), and the same is observed for the run-up signal on the left wall, therefore it is not shown here.

Finally, figure 25 shows the spatial profile of the wave crest envelope before the run-up on the right wall, i.e. the amplitude of the leading wave before the run-up, over the shoaling and run-up areas. One can identify the overshooting of Peregrine's and Nwogu's models, which overestimate wave amplitude up to the run-up (figure 25a). Except for MS and SGN equations, which underestimate wave amplitude, especially over the last kilometre, all other models are much closer to the reference solution. Most discrepancies appear over the last 20 m in figure 25b.

Apart from the run-up peak, fully nonlinear models better predict the wave train's evolution in this case. The SGN equations, fully nonlinear but with limited dispersion, give more accurate results than the dispersion-enhanced

Model	Instant of maximum run-up (s)	Maximum run-up height MRHRW (m)	Relative error on MRHRW w.r.t. whispers3D (%)
NSWE	1281.7	6.18	-74.7
Peregrine	1274.8	22.75	-6.8
SGN	1277.2	20.19	-17.3
MS	1276.9	17.41	-28.7
Nwogu	1275.0	23.17	-5.1
WKGS	1276.4	25.59	4.8
oKKCD	1276.5	24.41	0
diKKCD	1276.7	22.6	-7.4
eSGN	1276.5	20.52	-16
whispers3D	1276.5	24.41	

Table 5

Case 3 - Summary of time and height of the maximum run-up on the right wall for the different models.

weakly nonlinear models of Nwogu or MS. The enhanced eSGN equations, apart from propagating the shorter waves with a more accurate phase speed, give results similar to those obtained with the original SGN equations. Among the weakly nonlinear models, Nwogu's and Peregrine's models give almost identical results for the leading and highest waves and are the least accurate regarding the run-up signal, setting aside the first peak. This agrees with the findings of Filippini et al. (2015) that when nonlinear effects are significant, the behaviour of weakly nonlinear BT models only depends on whether they are formulated in amplitude-velocity form (spatial derivatives of the velocity in the momentum

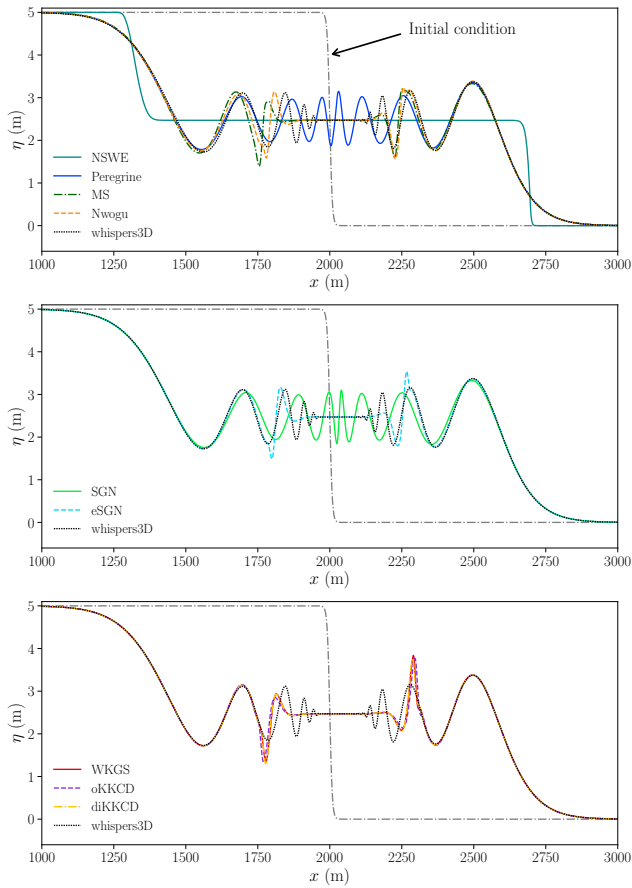


Figure 20: Case 3 - Free surface profiles at $t = 30$ s.

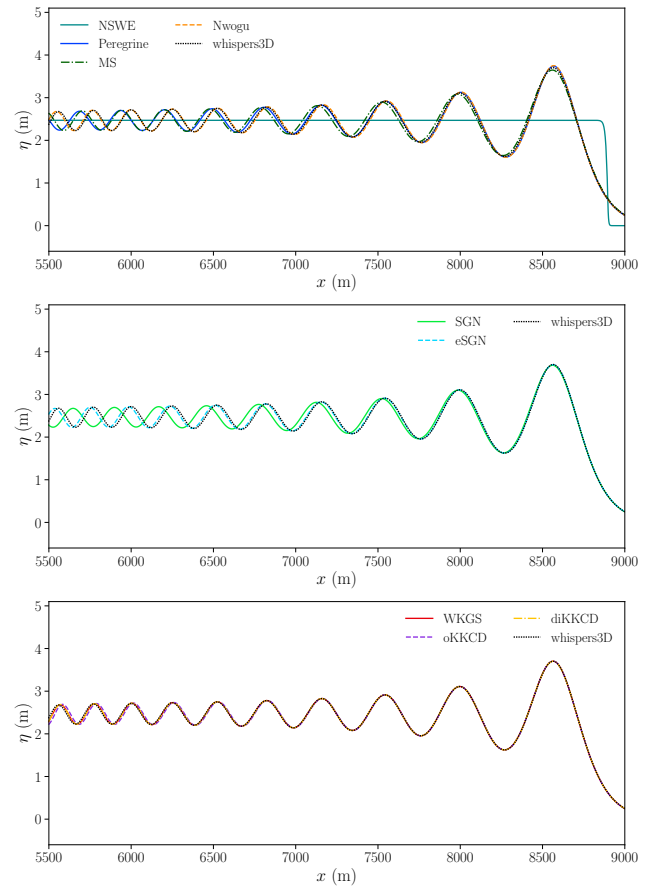


Figure 21: Case 3 - Free surface profiles at $t = 5$ min.

equation) or amplitude-flux form (derivatives of the flux). Improved models like the one from Nwogu give the same results as simpler models like Peregrine's since they are in amplitude-velocity form, while MS is in amplitude-flux form, explaining the two different behaviours. MS model gives the most differences regarding the MRHRW and the highest amplitude waves after shoaling, but the rest of the results are satisfactory. The WKGS model and the KKCD variants, particularly the oKKCD version, give very accurate results in this case, especially regarding the run-up peak and compared with eSGN.

6. Conclusion

In this work, eight variants of some weakly dispersive Boussinesq-type models among the most popular in the literature, either weakly or fully nonlinear, were compared. All models are reformulated with an auxiliary variable to deal with mixed space-time derivatives in the momentum equation, and an elliptic equation has to be solved at each time step to recover the representative horizontal velocity. These eight models are compared on three test cases of non-breaking long-wave propagation. The strong dispersive effects in case 1 allow us to discriminate between the improved models and the others. In cases 2 and 3, showing only weak to mild dispersive effects, few differences are observed

unless wave nonlinearity becomes important, which is the case mainly after the shoaling phase. We summarise here the main findings concerning the different models:

- Weakly nonlinear models: Peregrine's model cannot deal with the generation of high-order harmonics in case 1 due to its limited dispersion. In the other less dispersive cases, with a predominance of nonlinearity, it gives similar results to Nwogu's model despite their different dispersive characteristics, since they are both amplitude-velocity models. They generally predict overshooting and tend to overestimate wave and crest heights overall, including in the highly dispersive case 1 for Nwogu's model, although some underestimation is seen in case 2 and on the run-up peak in case 3. The MS model, however, systematically underestimates wave heights, leading also to some phase delay in case 3 despite its enhanced dispersive properties, and seems to give the worst results in all cases.
- Fully nonlinear models: Similarly to Peregrine's model, the insufficient dispersive properties of the original SGN equations prevent them from correctly modelling the propagation of the wave train in case 1. In the other cases, they give quite similar results as the MS model, with a significant underestimation of the

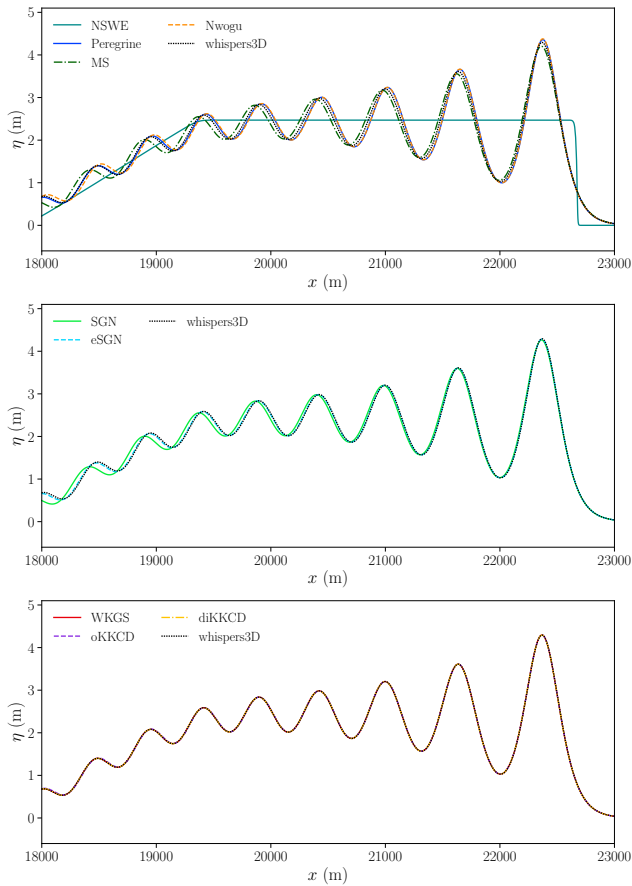


Figure 22: Case 3 - Free surface profiles at $t = 15$ min.

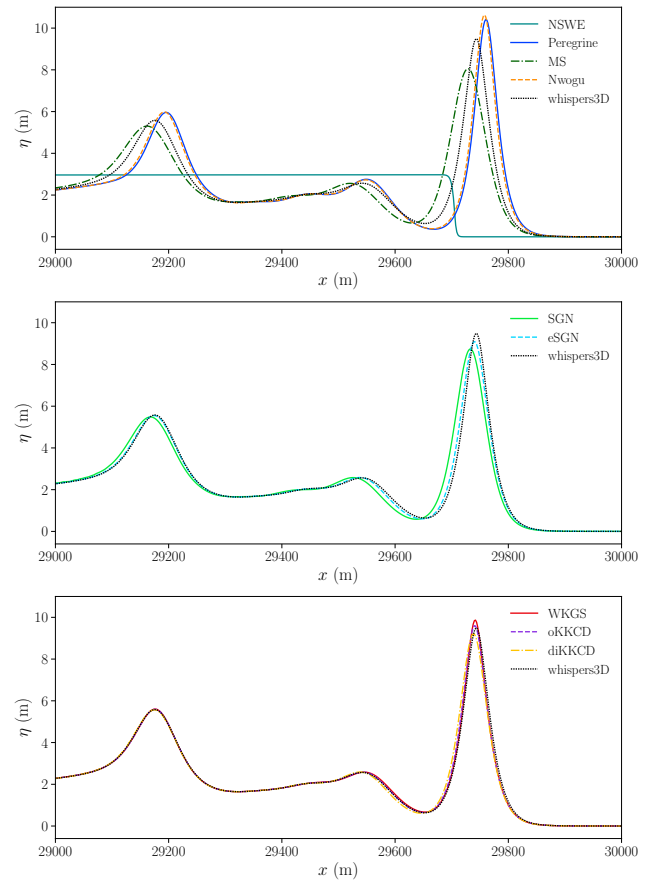


Figure 23: Case 3 - Free surface profiles at $t = 21$ min.

wave heights and crests. The eSGN equations with their enhanced dispersive properties underestimate only slightly less wave heights in cases 2 and 3, where nonlinearity prevails, but provide the best results of all models in case 1. All the variants of the WKGS and KKCD models give at least a little better results than eSGN in cases 2 and 3. Among them, the original WKGS equations appear to be the least accurate overall, overestimating wave heights in all 3 cases, in addition to the issues of significant overshooting mentioned in case 2. The diKKCD variant gives different results in case 1, but not obviously better, and shows somewhat similar performances in the other cases, underestimating wave heights similarly to eSGN yet to a lesser extent. One should also keep in mind that this model is the most stable out of the WKGS and KKCD variants and does not suffer from trough instabilities. oKKCD is the most accurate of all models in cases 2 and 3, giving almost identical results to diKKCD in case 1.

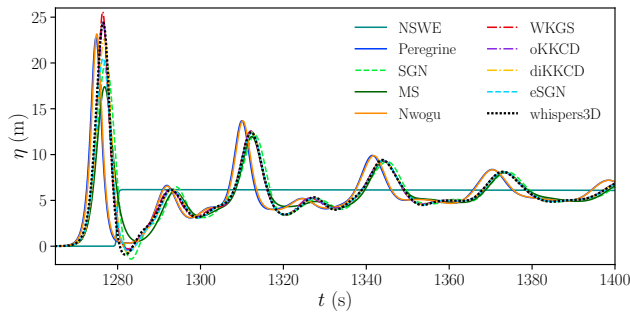
The superiority of fully nonlinear models may not appear obvious at first sight since, in nonlinear cases, the weakly nonlinear models of Nwogu (1993) and Peregrine (1967) give results somewhat closer to the reference than the variants of the SGN equations for instance. However, fully

nonlinear models appear more reliable and show consistent results in different situations, whereas weakly nonlinear models can behave differently. In particular, Peregrine's and Nwogu's models can either overestimate or underestimate wave height and run-up. To simulate wave propagation up to the shore, a wave-breaking model must be coupled to the weakly dispersive equations, with breaking detection criteria triggering energy dissipation mechanisms based on local wave parameters. Those criteria must be calibrated, which is rendered more difficult by the fact that weakly nonlinear models do not systematically predict correct wave heights or with the same tendencies compared to the reference.

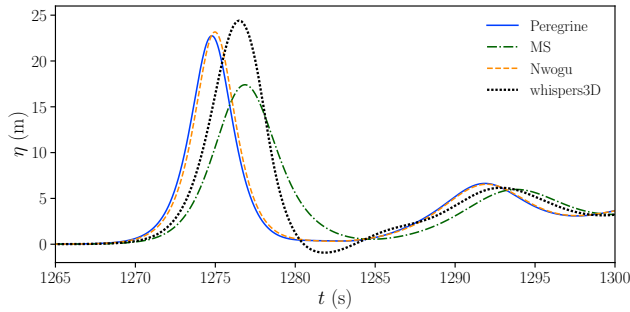
Among the eight BT variants investigated here, the fully nonlinear model of Kennedy et al. (2001) extending the model of Wei et al. (1995) with a time-varying reference elevation and using the optimal choice of parameters, referred to as oKKCD in this work, reveals the most accurate overall.

Acknowledgments

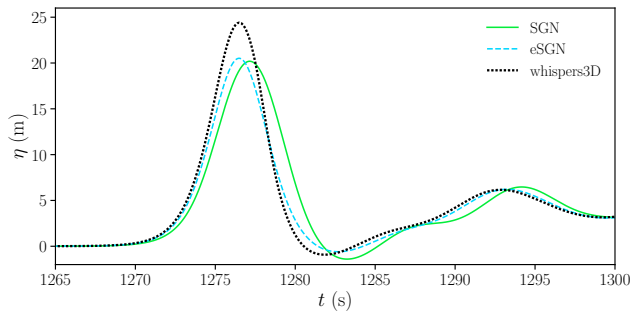
This work was carried out as part of EDF R&D's MOISE-2 research project on coastal and river flood hazard assessment, whose support the authors gratefully acknowledge. The authors also thank the French ANRT (Association



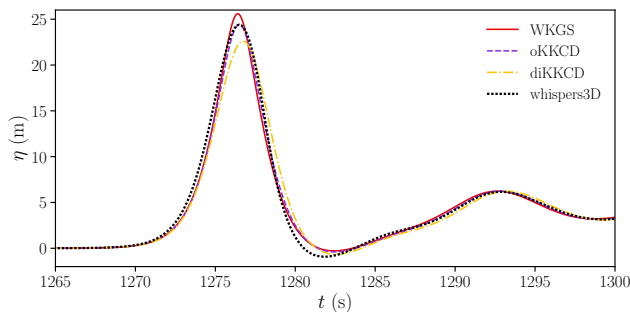
(a) Run-up of the first waves.



(b) Zoom on the run-up peak – Weakly nonlinear models.



(c) Zoom on the run-up peak – SGN models.



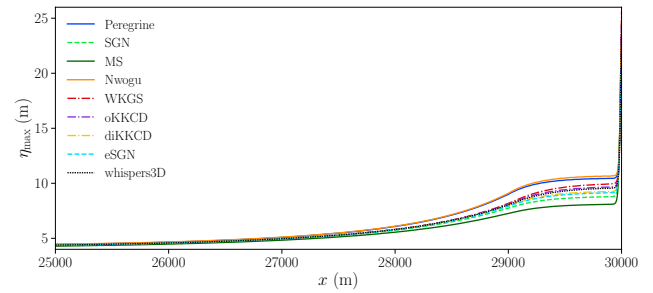
(d) Zoom on the run-up peak – WKGS and KKCD models.

Figure 24: Case 3 - Run-up signal on the right vertical wall.

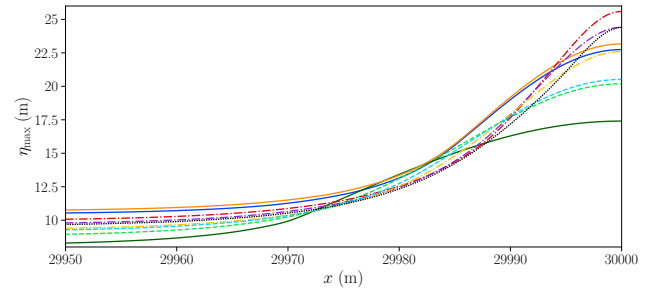
Nationale de la Recherche et de la Technologie) for its financial support towards Guillaume Coulaud's Ph.D. research program, through the CIFRE grant 2022/1017.

CRedit authorship contribution statement

Guillaume Coulaud: Investigation, Software, Formal Analysis, Visualization, Writing - original draft. **Maria**



(a) Shoaling and run-up regions (last 5 km of the domain).



(b) Zoom close to the right vertical wall (last 50 m of the domain).

Figure 25: Case 3 - Wave crest envelope for the shoaling and run-up phases.

Teles: Supervision, Writing - review and editing. **Michel Benoit:** Supervision, Conceptualization, Software, Writing - review and editing.

References

- Agnon, Y., Madsen, P.A., Schäffer, H.A., 1999. A new approach to high-order Boussinesq models. *Journal of Fluid Mechanics* 399, 319–333. doi:10.1017/S0022112099006394.
- Barré de Saint-Venant, A.J.C., 1871. Théorie du mouvement non permanent des eaux, avec application aux crues des rivières et à l'introduction de marées dans leur lit. *Comptes rendus de l'Académie des Sciences de Paris* 73, 147–154.
- Benoit, M., Dias, F., Herterich, J., Scolan, Y.M., 2018. Un Cas-Test Discriminant pour la Simulation de la Propagation et du Run-up de Trains de vagues de Type Tsunami, in: *Actes des 16èmes Journées de l'Hydrodynamique*, Marseille, France.
- Bonneton, P., Chazel, F., Lannes, D., Marche, F., Tissier, M., 2011. A splitting approach for the fully nonlinear and weakly dispersive Green-Naghdi model. *Journal of Computational Physics* 230, 1479–1498. doi:10.1016/j.jcp.2010.11.015.
- Boussinesq, J., 1872. Théorie des ondes et des remous qui se propagent le long d'un canal rectangulaire horizontal, en communiquant au liquide contenu dans ce canal des vitesses sensiblement pareilles de la surface au fond. *Journal de Mathématiques Pures et Appliquées* 17, 55–108.
- Brocchini, M., 2013. A reasoned overview on Boussinesq-type models: The interplay between physics, mathematics and numerics. *Proceedings of the Royal Society A: Mathematical, Physical and Engineering Sciences* 469, 20130496. doi:10.1098/rspa.2013.0496.
- Castro-Organ, O., Cantero-Chinchilla, F.N., Chanson, H., 2022. Shallow fluid flow over an obstacle: Higher-order non-hydrostatic modeling and breaking waves. *Environmental Fluid Mechanics* 22, 971–1003. doi:10.1007/s10652-022-09875-0.
- Chazel, F., Benoit, M., Ern, A., Piperno, S., 2009. A double-layer Boussinesq-type model for highly nonlinear and dispersive waves. *Proceedings of the Royal Society A: Mathematical, Physical and Engineering Sciences* 465, 2319–2346. doi:10.1098/rspa.2008.0508.

- Chazel, F., Lannes, D., Marche, F., 2011. Numerical Simulation of Strongly Nonlinear and Dispersive Waves Using a Green–Naghdi Model. *Journal of Scientific Computing* 48, 105–116. doi:10.1007/s10915-010-9395-9.
- Chen, Y., Liu, P.L.F., 1995. Modified Boussinesq equations and associated parabolic models for water wave propagation. *Journal of Fluid Mechanics* 288, 351–381. doi:10.1017/S0022112095001170.
- Choi, J., Kirby, J.T., Yoon, S.B., 2015. Reply to “Discussion to ‘Boussinesq modeling of longshore currents in the Sandy Duck experiment under directional random wave conditions’ by J. Choi, J. T. Kirby and S.B. Yoon”. *Coastal Engineering* 106, 4–6. doi:10.1016/j.coastaleng.2015.09.002.
- Cienfuegos, R., Barthélemy, E., Bonneton, P., 2006. A fourth-order compact finite volume scheme for fully nonlinear and weakly dispersive Boussinesq-type equations. Part I: model development and analysis. *International Journal for Numerical Methods in Fluids* 51, 1217–1253. doi:10.1002/flid.1141.
- Clamond, D., Dutykh, D., Mitsotakis, D., 2017. Conservative modified Serre–Green–Naghdi equations with improved dispersion characteristics. *Communications in Nonlinear Science and Numerical Simulation* 45, 245–257. doi:10.1016/j.cnsns.2016.10.009.
- Dingemans, M.W., 1994. Comparison of Computations with Boussinesq-like Models and Laboratory Measurements. Technical Report MAST-G8M Note H1684.12. Delft Hydraulics.
- Dingemans, M.W., 1997. Water Wave Propagation Over Uneven Bottoms: Part 1. volume 13 of *Advanced Series on Ocean Engineering*. World Scientific Publishing Company. doi:10.1142/1241-part1.
- Duran, A., Marche, F., 2017. A discontinuous Galerkin method for a new class of Green–Naghdi equations on simplicial unstructured meshes. *Applied Mathematical Modelling* 45, 840–864. doi:10.1016/j.apm.2017.01.030.
- Dutykh, D., Clamond, D., Milewski, P., Mitsotakis, D., 2013. Finite volume and pseudo-spectral schemes for the fully nonlinear 1D Serre equations. *European Journal of Applied Mathematics* 24, 761–787. doi:10.1017/S0956792513000168.
- Eldrup, M.R., Lykke Andersen, T., 2020. Numerical Study on Regular Wave Shoaling, De-Shoaling and Decomposition of Free/Bound Waves on Gentle and Steep Foreshores. *Journal of Marine Science and Engineering* 8, 334. doi:10.3390/jmse8050334.
- Filippini, A.G., 2016. Free Surface Flow Simulation in Estuarine and Coastal Environments : Numerical Development and Application on Unstructured Meshes. Ph.D. thesis. Université de Bordeaux.
- Filippini, A.G., Bellec, S., Colin, M., Ricchiuto, M., 2015. On the nonlinear behaviour of Boussinesq type models: Amplitude-velocity vs amplitude-flux forms. *Coastal Engineering* 99, 109–123. doi:10.1016/j.coastaleng.2015.02.003.
- Filippini, A.G., Kazolea, M., Ricchiuto, M., 2016. A flexible genuinely nonlinear approach for nonlinear wave propagation, breaking and run-up. *Journal of Computational Physics* 310, 381–417. doi:10.1016/j.jcp.2016.01.027.
- Gobbi, M.F., Kirby, J.T., 1999. Wave evolution over submerged sills: Tests of a high-order Boussinesq model. *Coastal Engineering* 37, 57–96. doi:10.1016/S0378-3839(99)00015-0.
- Gobbi, M.F., Kirby, J.T., Wei, G., 2000. A fully nonlinear Boussinesq model for surface waves. Part 2. Extension to $O(kh)^4$. *Journal of Fluid Mechanics* 405, 181–210. doi:10.1017/S0022112099007247.
- Green, A.E., Naghdi, P.M., 1976. A derivation of equations for wave propagation in water of variable depth. *Journal of Fluid Mechanics* 78, 237–246. doi:10.1017/S0022112076002425.
- Kazolea, M., Delis, A.I., 2013. A well-balanced shock-capturing hybrid finite volume–finite difference numerical scheme for extended 1D Boussinesq models. *Applied Numerical Mathematics* 67, 167–186. doi:10.1016/j.apnum.2011.07.003.
- Kazolea, M., Delis, A.I., Nikolos, I.K., Synolakis, C.E., 2012. An unstructured finite volume numerical scheme for extended 2D Boussinesq-type equations. *Coastal Engineering* 69, 42–66. doi:10.1016/j.coastaleng.2012.05.008.
- Kazolea, M., Delis, A.I., Synolakis, C.E., 2014. Numerical treatment of wave breaking on unstructured finite volume approximations for extended Boussinesq-type equations. *Journal of Computational Physics* 271, 281–305. doi:10.1016/j.jcp.2014.01.030.
- Kazolea, M., Filippini, A.G., Ricchiuto, M., Abadie, S., Martin Medina, M., Morichon, D., Journeau, C., Marcer, R., Pons, K., LeRoy, S., Pedreros, R., Rousseau, M., 2019. Wave propagation, breaking, and overtopping on a 2D reef: A comparative evaluation of numerical codes for tsunami modelling. *European Journal of Mechanics - B/Fluids* 73, 122–131. doi:10.1016/j.euromechflu.2017.10.010.
- Kazolea, M., Filippini, A.G., Ricchiuto, M., 2023. Low dispersion finite volume/element discretization of the enhanced Green–Naghdi equations for wave propagation, breaking and runup on unstructured meshes. *Ocean Modelling* 182, 102157. doi:10.1016/j.ocemod.2022.102157.
- Kazolea, M., Ricchiuto, M., 2018. On wave breaking for Boussinesq-type models. *Ocean Modelling* 123, 16–39. doi:10.1016/j.ocemod.2018.01.003.
- Kazolea, M., Ricchiuto, M., 2024. Full Nonlinearity in Weakly Dispersive Boussinesq Models: Luxury or Necessity. *Journal of Hydraulic Engineering* 150, 04023061. doi:10.1061/JHEND8.HYENG-13718.
- Kennedy, A.B., Chen, Q., Kirby, J.T., Dalrymple, R.A., 2000. Boussinesq Modeling of Wave Transformation, Breaking, and Runup. I: 1D. *Journal of Waterway, Port, Coastal, and Ocean Engineering* 126, 39–47. doi:10.1061/(ASCE)0733-950X(2000)126:1(39).
- Kennedy, A.B., Kirby, J.T., Chen, Q., Dalrymple, R.A., 2001. Boussinesq-type equations with improved nonlinear performance. *Wave Motion* 33, 225–243. doi:10.1016/S0165-2125(00)00071-8.
- Kim, G., Lee, C., Suh, K.D., 2007. Internal generation of waves: Delta source function method and source term addition method. *Ocean Engineering* 34, 2251–2264. doi:10.1016/j.oceaneng.2007.06.002.
- Kirby, J.T., 2003. Boussinesq models and applications to nearshore wave propagation, surf zone processes and wave-induced currents, in: Lakkan, V.C. (Ed.), *Advances in Coastal Modeling*. Elsevier. volume 67 of *Elsevier Oceanography Series*, pp. 1–41.
- Kirby, J.T., 2016. Boussinesq Models and Their Application to Coastal Processes across a Wide Range of Scales. *Journal of Waterway, Port, Coastal, and Ocean Engineering* 142, 03116005. doi:10.1061/(ASCE)WW.1943-5460.0000350.
- Kirby, J.T., 2020. A new instability for Boussinesq-type equations. *Journal of Fluid Mechanics* 894, F1. doi:10.1017/jfm.2020.257.
- Lannes, D., Marche, F., 2015. A new class of fully nonlinear and weakly dispersive Green–Naghdi models for efficient 2D simulations. *Journal of Computational Physics* 282, 238–268. doi:10.1016/j.jcp.2014.11.016.
- Le Métayer, O., Gavriluk, S., Hank, S., 2010. A numerical scheme for the Green–Naghdi model. *Journal of Computational Physics* 229, 2034–2045. doi:10.1016/j.jcp.2009.11.021.
- Lee, C., Cho, Y.S., Yoon, S.B., 2003. A note on linear dispersion and shoaling properties in extended Boussinesq equations. *Ocean Engineering* 30, 1849–1867. doi:10.1016/S0029-8018(03)00015-5.
- Li, M., Xu, L., Cheng, Y., 2019. A CDG-FE method for the two-dimensional Green–Naghdi model with the enhanced dispersive property. *Journal of Computational Physics* 399, 108953. doi:10.1016/j.jcp.2019.108953.
- Liu, Z., Fang, K., 2016. A new two-layer Boussinesq model for coastal waves from deep to shallow water: Derivation and analysis. *Wave Motion* 67, 1–14. doi:10.1016/j.wavemoti.2016.07.002.
- Liu, Z.B., Fang, K.Z., Cheng, Y.Z., 2018. A new multi-layer irrotational Boussinesq-type model for highly nonlinear and dispersive surface waves over a mildly sloping seabed. *Journal of Fluid Mechanics* 842, 323–353. doi:10.1017/jfm.2018.99.
- Lteif, R., 2024. An operator-splitting approach with a hybrid finite volume/finite difference scheme for extended Boussinesq models. *Applied Numerical Mathematics* 196, 159–182. doi:10.1016/j.apnum.2023.10.009.
- Lynett, P.J., Liu, P.L.F., 2004. A two-layer approach to wave modelling. *Proceedings of the Royal Society of London. Series A: Mathematical, Physical and Engineering Sciences* 460, 2637–2669. doi:10.1098/rspa.2004.1305.
- Madsen, P., Banijamali, B., Schäffer, H., Sørensen, O., 1997a. Boussinesq Type Equations with High Accuracy in Dispersion and Nonlinearity, in: *Proceedings of 25th International Conference on Coastal Engineering*

- 1996, American Society of Civil Engineers, Orlando, Florida, United States. pp. 95–108. doi:10.1061/9780784402429.008.
- Madsen, P.A., Bingham, H.B., Liu, H., 2002. A new Boussinesq method for fully nonlinear waves from shallow to deep water. *Journal of Fluid Mechanics* 462, 1–30. doi:10.1017/S0022112002008467.
- Madsen, P.A., Bingham, H.B., Schäffer, H.A., 2003. Boussinesq-type formulations for fully nonlinear and extremely dispersive water waves: Derivation and analysis. *Proceedings of the Royal Society of London. Series A: Mathematical, Physical and Engineering Sciences* 459, 1075–1104. doi:10.1098/rspa.2002.1067.
- Madsen, P.A., Fuhrman, D.R., 2020. Trough instabilities in Boussinesq formulations for water waves. *Journal of Fluid Mechanics* 889, A38. doi:10.1017/jfm.2020.76.
- Madsen, P.A., Schäffer, H.A., 1998. Higher-order Boussinesq-type equations for surface gravity waves: Derivation and analysis. *Philosophical Transactions of the Royal Society of London. Series A: Mathematical, Physical and Engineering Sciences* 356, 3123–3181. doi:10.1098/rsta.1998.0309.
- Madsen, P.A., Schäffer, H.A., 1999. A review of Boussinesq-type equations for surface gravity waves. *Advances in Coastal and Ocean Engineering* 5, 1–94. doi:10.1142/9789812797544_0001.
- Madsen, P.A., Sørensen, O.R., 1992. A new form of the Boussinesq equations with improved linear dispersion characteristics. Part 2. A slowly-varying bathymetry. *Coastal Engineering* 18, 183–204. doi:10.1016/0378-3839(92)90019-0.
- Madsen, P.A., Sørensen, O.R., Schäffer, H.A., 1997b. Surf zone dynamics simulated by a Boussinesq type model. Part II: Surf beat and swash oscillations for wave groups and irregular waves. *Coastal Engineering* 32, 289–319. doi:10.1016/S0378-3839(97)00029-X.
- Mase, H., Kirby, J.T., 1992. Hybrid Frequency-Domain KdV Equation for Random Wave Transformation, in: *Proceedings of 23rd International Conference on Coastal Engineering 1992*, American Society of Civil Engineers, Venice, Italy. pp. 474–487. doi:10.1061/9780872629332.035.
- Mei, C.C., Le Méhauté, B., 1966. Note on the equations of Long waves over an uneven bottom. *Journal of Geophysical Research (1896-1977)* 71, 393–400. doi:10.1029/JZ071i002p00393.
- Mihami, F.Z., 2023. Development of a Phase-resolving Computer Model for Operational Nearshore Wave Assessment. Ph.D. thesis. Université de Pau et des Pays de l'Adour. France.
- Mitsotakis, D., Synolakis, C., McGuinness, M., 2017. A modified Galerkin/finite element method for the numerical solution of the Serre-Green-Naghdi system. *International Journal for Numerical Methods in Fluids* 83, 755–778. doi:10.1002/flid.4293.
- Neossi Nguetchue, S.N., Abelman, S., 2008. A computational algorithm for solving nearly penta-diagonal linear systems. *Applied Mathematics and Computation* 203, 629–634. doi:10.1016/j.amc.2008.05.012.
- Nwogu, O., 1993. Alternative Form of Boussinesq Equations for Nearshore Wave Propagation. *Journal of Waterway, Port, Coastal, and Ocean Engineering* 119, 618–638. doi:10.1061/(ASCE)0733-950X(1993)119:6(618).
- Nwogu, O., Demirbilek, Z., 2001. BOUSS-2D: A Boussinesq Wave Model for Coastal Regions and Harbors. Technical Report TR-01-25. ERDC/CHL.
- Panda, N., Dawson, C., Zhang, Y., Kennedy, A.B., Westerink, J.J., Donahue, A.S., 2014. Discontinuous Galerkin methods for solving Boussinesq-Green-Naghdi equations in resolving non-linear and dispersive surface water waves. *Journal of Computational Physics* 273, 572–588. doi:10.1016/j.jcp.2014.05.035.
- Peregrine, D.H., 1967. Long waves on a beach. *Journal of Fluid Mechanics* 27, 815–827. doi:10.1017/S0022112067002605.
- Pitt, J.P., Zoppou, C., Roberts, S.G., 2021. Solving the fully nonlinear weakly dispersive Serre equations for flows over dry beds. *International Journal for Numerical Methods in Fluids* 93, 24–43. doi:10.1002/flid.4873.
- Roeber, V., Cheung, K.F., 2012. Boussinesq-type model for energetic breaking waves in fringing reef environments. *Coastal Engineering* 70, 1–20. doi:10.1016/j.coastaleng.2012.06.001.
- Serre, F., 1953. Contribution to the study of permanent and non-permanent flows in channels. *La Houille Blanche* 39, 830–872. doi:10.1051/lhb/1953058.
- Shi, F., Kirby, J.T., Harris, J.C., Geiman, J.D., Grilli, S.T., 2012. A high-order adaptive time-stepping TVD solver for Boussinesq modeling of breaking waves and coastal inundation. *Ocean Modelling* 43–44, 36–51. doi:10.1016/j.ocemod.2011.12.004.
- Su, C.H., Gardner, C.S., 1969. Korteweg-de Vries Equation and Generalizations. III. Derivation of the Korteweg-de Vries Equation and Burgers Equation. *Journal of Mathematical Physics* 10, 536–539. doi:10.1063/1.1664873.
- Tonelli, M., Petti, M., 2009. Hybrid finite volume – finite difference scheme for 2DH improved Boussinesq equations. *Coastal Engineering* 56, 609–620. doi:10.1016/j.coastaleng.2009.01.001.
- Wei, G., Kirby, J.T., Grilli, S.T., Subramanya, R., 1995. A fully nonlinear Boussinesq model for surface waves. Part 1. Highly nonlinear unsteady waves. *Journal of Fluid Mechanics* 294, 71–92. doi:10.1017/S0022112095002813.
- Wei, G., Kirby, J.T., Sinha, A., 1999. Generation of waves in Boussinesq models using a source function method. *Coastal Engineering* 36, 271–299. doi:10.1016/S0378-3839(99)00009-5.
- Yang, Z., Liu, P.L.F., 2022. Depth-integrated wave-current models. Part 2. Current with an arbitrary profile. *Journal of Fluid Mechanics* 936, A31. doi:10.1017/jfm.2022.42.
- Yang, Z.T., Liu, P.L.F., 2020. Depth-integrated wave-current models. Part 1. Two-dimensional formulation and applications. *Journal of Fluid Mechanics* 883, A4. doi:10.1017/jfm.2019.831.
- Zhang, J., Benoit, M., 2021. Wave-bottom interaction and extreme wave statistics due to shoaling and de-shoaling of irregular long-crested wave trains over steep seabed changes. *Journal of Fluid Mechanics* 912, A28. doi:10.1017/jfm.2020.1125.
- Zhang, J., Benoit, M., Kimmoun, O., Chabchoub, A., Hsu, H.C., 2019. Statistics of Extreme Waves in Coastal Waters: Large Scale Experiments and Advanced Numerical Simulations. *Fluids* 4, 99. doi:10.3390/fluids4020099.
- Zhang, J., Benoit, M., Ma, Y., 2022. Equilibration process of out-of-equilibrium sea-states induced by strong depth variation: Evolution of coastal wave spectrum and representative parameters. *Coastal Engineering* 174, 104099. doi:10.1016/j.coastaleng.2022.104099.
- Zoppou, C., Pitt, J., Roberts, S.G., 2017. Numerical solution of the fully non-linear weakly dispersive serre equations for steep gradient flows. *Applied Mathematical Modelling* 48, 70–95. doi:10.1016/j.apm.2017.03.059.